# Cellular senescence inhibits renal regeneration after injury in mice, with senolytic treatment promoting repair

**Title:**

Cellular senescence inhibits renal regeneration after injury in mice, and senolytic treatment promotes repair

**One Sentence summary:**

Senescent renal epithelia promote fibrosis and functional loss after injury whereas depletion improves regeneration in aged or irradiated kidneys.

**Authors**

Katie J Mylonas[1], Eoin D O'Sullivan[1], Duncan Humphries[1], David P Baird[1,2], Marie-Helena Docherty[1], Sarah A Neely[1,3], Paul J Krimpenfort[4], Anette Melk[5], Roland Schmitt[5], Sofia Ferreira-Gonzalez [3], Stuart J Forbes[3], Jeremy Hughes[1] and David A Ferenbach[1*]

**Affiliations**

[1]Centre for Inflammation Research, Queen's Medical Research Institute, University of Edinburgh, Edinburgh EH16 4TJ, UK.

[2]Royal Infirmary of Edinburgh, Edinburgh EH16 4SA, UK

[3]Centre for Regenerative Medicine, University of Edinburgh, Edinburgh EH16 4UU, UK

[4]Netherlands Cancer Institute, 1066 CX Amsterdam, Netherlands

[5]Hannover Medical School, 30625 Hannover, Germany

*Corresponding author

**Abstract**

The ability of the kidney to regenerate successfully after injury is lost with advancing age, chronic kidney disease and after irradiation. The factors responsible for this reduced regenerative capacity remain incompletely understood, with increasing interest in a potential role for cellular senescence in determining outcomes after injury. Here, we demonstrated correlations between senescent cell load and functional loss in human aging and chronic kidney diseases including radiation nephropathy. We dissected the causative role of senescence in the augmented fibrosis occurring after injury in aged and irradiated murine kidneys. In vitro studies on human proximal tubular epithelial cells, and in vivo mouse studies demonstrated that senescent renal epithelial cells produced multiple components of the senescence associated secretory phenotype including transforming growth factor beta-1, induced fibrosis and inhibited tubular proliferative capacity after injury. Treatment of aged and irradiated mice with the B-cell lymphoma (Bcl) 2/w/xL inhibitor ABT-263 reduced senescent cell numbers and restored a regenerative phenotype in the kidneys with increased tubular proliferation, improved function and reduced fibrosis after subsequent ischaemia-reperfusion injury. Senescent cells are key determinants of renal regenerative capacity in mice and represent emerging treatment targets to protect aging and vulnerable kidneys in man.

## Introduction

Hundreds of millions of people worldwide live with chronic kidney disease (CKD), a condition characterised by progressive kidney fibrosis, renal functional decline and premature cardiovascular death (*1*). CKD prevalence is increasing, and aging adults (>65 years old) are known to be at particular risk (*2*). Aging adults and patients with CKD are also more susceptible to acute kidney injury (AKI), a life-threatening complication which itself can accelerate progression of underlying renal fibrosis and loss of function (*3*). Therefore, incompletely understood factors in the aging and chronically injured kidney promote fibrosis and inhibit renal regeneration. Understanding these processes and modifying them to protect vulnerable aging and injured kidneys represents an unmet research and clinical need.

Senescent cells (SCs) are permanently growth arrested and phenotypically altered cells which accumulate in vivo with aging, organ injury and after genotoxic insults such as ionizing radiation. Senescence is associated with worsened damage and reduced regenerative capacity following tissue injury (*4-6*). Recent evidence implicated SC accumulation as contributing to aging and age-related diseases in fast-aging and naturally aged mice, with depletion strategies extending healthy lifespan (*7, 8*). SCs have also been reported to be present in increased numbers in human and rodent kidneys with aging, CKD and after transplantation (*9-12*). Whether SCs actively contribute to the increased fibrosis and reduced regenerative capacity seen in aged and injured kidneys subject to further injury is a topic of major clinical and research interest(*13*).

SCs are attractive therapeutic targets as they remain metabolically active with constitutive nuclear factor kappa-light-chain-enhancer of activated B cells (NF-kB) activation driving

expression of the senescence-associated secretory phenotype (SASP) with release of cytokines (Interleukin (IL)-6, Tumour necrosis factor (TNF-α), chemokines (chemokine (C-C motif) ligand (CCL)2, chemokine (C-X-C motif) ligand CXCL8) and pro-fibrotic transforming growth factor beta (TGF)-β (*14*). ABT-263, a potent B-cell lymphoma (Bcl)2/w/xL inhibitor, effectively depletes SCs when administered orally to irradiated or normally aged mice (*15*). Depletion reduces irradiation-induced premature haematopoietic aging and rejuvenates aged tissue stem cells (*15*). The efficacy of ABT-263 treatment on kidney regeneration and fibrosis after injury in aged animals and animals with prematurely senescent kidneys (via total body irradiation, TBI) remains untested.

In this study, we tested the hypothesis that senescent renal epithelia are key determinants of fibrosis and regenerative capacity after renal injury and can be therapeutically targeted. Senescent proximal tubular epithelial cells (PTECs) were identified in naturally aged mice, were also induced by radiation exposure in vitro and in vivo and were depleted using ABT-263. By doing so, we demonstrate the importance of epithelial senescence in kidney fibrosis, damage response, function and repair after injury, as well as the impact of their depletion on successful regeneration.

## Results

**Markers of renal senescence are increased in patients with age and chronic kidney disease.** Using two separate human datasets of renal transcriptomic data available on the *Nephroseq* repository (*16, 17*), we determined expression of markers of permanent cell cycle arrest in healthy and diseased kidneys using *CDKN1A* (P21CIP1) and *CDKN2A* (P16INK4A) expression (Fig 1A). Both *CDKN1A* and *CDKN2A* were increased in diseased kidneys vs healthy controls (Fig 1B; *CDKN1A*: $p=5.52x10^{-9}$, *CDKN2A*: $p=1.2x10^{-8}$; based on median centred Log2 expression) and rose progressively with age, with *CDKN1A* expressed more highly (Fig 1C; p=0.004; CDKN2A p=0.048). Of note, only *CDKN1A* was significantly associated with falling kidney function in chronic kidney disease (measured by estimated renal glomerular filtration rate; eGFR) (Fig 1D; p=0.0015); validating *CDKN1A* as a marker of both age- and injury-related renal senescence. Multivariate regression demonstrated that age and eGFR were independently associated with changes in CDKN1A whereas the univariable models associations of age with CDKN2A was lost in the multivariable model (table S1). The transcriptome analysis of kidney biopsies in human CKD patients and healthy donors also identified upregulation in multiple transcripts of members of the SASP, fibrosis and BCL family members (Fig. S1)

Immunohistochemistry (IHC) staining of a local Edinburgh dataset performed in our United Kingdom Accreditation Service (UKAS)-certified histology lab demonstrated that nuclear P21CIP1 staining was induced in diseased kidneys versus healthy controls (Fig 1E; $p<0.05$). Immunohistochemistry for P16INK4A and P21CIP1 demonstrated minimal staining in the young healthy kidney but increased P21CIP1 expression was detected in disease [early glomerulonephritis, radiation nephropathy and in advanced renal fibrosis (Fig 1F)]. In each

case P21CIP1 staining appeared confined to tubular epithelia, in contrast to P16INK4A which was expressed at much lower concentrations in epithelial and interstitial cells (Fig 1G-H).

**ABT-263 specifically targets senescent human renal proximal tubular epithelial cells (RPTECs).** Human RPTECs exposed in vitro to 10 Gray (Gy) γ-radiation developed reduced total cell number ($p<0.05$) and increased cell size ($p<0.05$) compared to non-irradiated controls (Fig 2A-C), consistent with induction of senescence. Quantitative polymerase chain reaction (qPCR) analysis at d7 post-irradiation revealed significantly decreased proliferation as measured by *MKI67* (KI67) expression ($p<0.005$), loss of *LMNB1* (Lamin B1; $p<0.05$), increased cyclin dependent kinase inhibitors *CDKN2A* ($p<0.05$) and *CDKN1A* (P21CIP1; $p<0.005$) and increases in SASP markers *IL1B (p<0.05)*, *TNF (p<0.05)* and *TGFB1 (p<0.0005), MMP1* (matrix metalloprotease 1) and neutrophil chemotactic factor, *CXCL8* (Fig 2D). Because ABT-263 targets BCL-2 family members, *BCL2* (BCL-2*)*, *BCL2L1* (BCL-xl) and *BCL2L2* (BCl-w) were measured and all demonstrated increased mRNA expression in irradiated/senescent RPTECs vs control (Fig 2d; *BCL2;* $p< 0.01$, *BCL2L;* $p< 0.01$ and *BCL2L2;* $p< 0.01$). Irradiated RPTECs also increased senescence-associated (SA)-β-Galactosidase expression (Fig 2E, $p<0.001$). Collectively these findings indicated that 10Gy irradiation induces senescence and its associated secretory phenotype in human RPTECs.

We then tested the specificity of ABT-263 to induce cell death in human senescent RPTECs. ABT-263 selectively killed senescent cells in a dose-dependent manner, with higher concentrations of ABT-263 (1μM and 5μM), reducing viable SCs to 2% and 0% (relative to vehicle-treated SCs) (Fig 2F). There was no toxicity to non-irradiated cells at even the highest concentrations of ABT263 (Fig 2F), which was unexpected, as previous studies had

found some toxicity at higher concentrations in non-senescent human renal epithelial cells(*15*).

**Aged mice have higher expression of SASP factors and worsened fibrotic responses after IRI.** Baseline expression senescence/fibrosis in kidneys of old and young mice were measured (Fig 3A). qPCR analysis revealed upregulation of senescence-associated *Cdkn1a* (P21CIP1; $p<0.05$), *Cdkn2a* ($p<0.005$), as well as SASP genes (*Il6;* $p<0.05$, *Tnf;* $p<0.01$, *Tgfb1;* $p<0.05$) in old compared with young kidneys (Fig 3B). Fibrosis, as measured by Collagen I immunofluorescence (IF) was higher in old kidneys ($p<0.01$; Fig 3C) with an equivalent rise in total Collagen seen on picrosirius red (PSR) staining ($p<0.05$; Fig 3D). γH2A.X staining showed evidence of increased DNA damage and DNA damage response (DDR) in the outer medulla and cortex of old kidneys compared to the young kidneys (Fig 3E). Lamin B1 antibody IF was performed, confirming that Lamin B1 was lost in kidney tubular nuclei with age (Fig 3F). To assess the impact of age on renal regeneration after injury the outcome of unilateral ischemia reperfusion injury (IRI) was tested in old and young mice (Fig 3G), demonstrating that old mice develop greater fibrosis after identical durations of injury ($p<0.005$; Fig 3H), with IRI resulting in an increase in expression of senescence-associated *Cdkn1a* by qPCR ($p<0.01$; Fig 3I).

**Clearance of SC in aged mice protects the kidney after AKI.** To test whether pre-existing SCs present at increased numbers in old animals promote fibrosis and inhibit regeneration after subsequent AKI, old female mice were treated with ABT-263 to deplete SCs before unilateral IRI surgery (Fig 4A). 5 weeks after IRI kidneys were harvested and analysed. Senolytic pre-treatment significantly reduced the numbers of senescent cells present in the uninjured injury ($p<0.05$; Fig S2A) and reduced post-IRI fibrosis ($p<0.01$; Fig S2B-C)

Key markers of senescence, SASP release and *Bcl2* family transcripts were measured by qPCR, compared to old naïve kidneys (with naïve kidney expression shown by the red line, Fig. 4B and S2D). These demonstrated induction of multiple senescence-associated transcripts, with *Cdkn1a* expression reduced by ABT-263 treatment (Fig 4B) and *Bcl2l2* (BCL-W; $p<0.05$) also showing reduction. Post-ischaemic kidney weight (vs the contralateral kidney from the same mouse, Fig 4C) was increased in senolytic-treated compared to control treated animals, although this remained below healthy weight (shown by red line). Given that IRI leads to tubular loss (*19*), this implicated senescent cells in impeding tubular recovery and survival after injury, with senolytic treatment potentially restoring regenerative capacity by increasing proliferative capacity in remaining renal tubules (*20*). To dissect these processes, further experiments were undertaken.

Kidney Injury Molecule 1 (KIM-1/*Havcr1*) is upregulated acutely in damaged proximal tubules in humans (*21*) and chronic expression in CKD predicts likelihood of progression to end stage-renal disease (ESRD) in man (*22*). We quantified KIM-1 protein 5 weeks post-IRI as a marker of ongoing tubular injury and progressive fibrosis in diseased kidneys. KIM-1 was reduced in ABT-263-treated IRI vs vehicle-treated IRI kidneys ($p<0.01$; Fig 4D), illustrating that senescent tubular cells drive chronic KIM-1 release in diseased kidneys, and their depletion in vivo was safe and opposed ongoing injury. Haemotoxylin and eosin (H&E) staining revealed improved renal architecture in ABT-263 vs vehicle-treated mice (Fig S2E).

Kidney sections were then stained with *Lotus tetragonolobus* lectin (LTL), a marker of differentiated renal tubules (*23*) and the proliferation marker Ki67 (Fig 4E-F). IRI induces loss of tubules (*19*). Proliferating KI67+ LTL+ tubules were counted (Fig 4F; white arrows in

Fig 4E). ABT-263 pre-treated old IRI kidneys exhibited significantly increased tubular proliferation compared to control ($p<0.01$; Fig 4F). Thus, senescence inhibits epithelial proliferation in response to injury. As TGF-β1 is a recognised driver of renal fibrosis post-IRI (*24-26*) and is produced by SC (*27, 28*), this protein was measured in the kidney. Senolytic treatment reduced TGF-β1 in diseased kidneys ($p<0.05$; Fig 4G), consistent with a role of senescent epithelia in controlling renal TGF-β1 through direct production ± recruitment of TGF-β1 producing cells. TGF-β1 is thought to drive renal fibrosis in part through mediating macrophage infiltration and switching to a pro-fibrotic CD206+ phenotype (*26, 29*). ABT-263 treatment reduced the overall number of F480+ macrophages ($p<0.05$; Fig S2G-H) and percentage of F480+/CD206+ macrophages in the post-IRI diseased kidney ($p<0.01$; Fig S2I). Therefore, senescence affects macrophage phenotype in post-IRI kidney disease, increasing pro-fibrotic CD206+ macrophages. Whereas SA-β-galactosidase was not reduced (Fig S2J), a marked reduction in yH2A.X foci in the cortex ($p<0.05$; Fig S2K) and increase in Lamin B1-positive nuclei ($p<0.01$; Fig S2L) were both noted with ABT-263 treatment .

To establish whether the improvement in multiple markers of senescence and fibrosis translated into enhanced renal functional recovery after IRI, further experiments used a bilateral IRI injury to generate a model of functional kidney injury and impairment (Figure 5A). Aged mice treated with ABT-263 prior to bilateral IRI had significantly improved renal function measured by serum Cystatin C ($p<0.01$ at both d7 and 14; Fig 5B) and reduced numbers of p21CIP1+ senescent cells prior to injury ($p<0.05$; Fig 5C). This functional protection was accompanied by reduced renal fibrosis by both PSR staining ($p<0.01$; Fig 5D-E) and Collagen I analysis by immunflorescence ($p<0.01$; Fig 5F-G). Hence, senescent cell depletion improves the subsequent structural and functional regenerative capacity of the naturally aged kidney.

**Total body irradiation induces cellular senescence and fibrosis in the murine kidney in vivo.** To distinguish the specific effects of senescence from those of the general aging phenotype, γ-irradiation was used to induce senescence in the young murine kidney (*15*). Young C57BL/6 mice underwent 7Gy total body irradiation (TBI) with tissue harvest 8 and 16 weeks later (Fig 6A), with imaging of whole kidneys to determine patterns of DNA damage by γH2A.X staining (Fig 6B-C). qPCR analysis of kidneys showed that the senescence marker *Cdkn1a* (P21CIP1) increased over time after TBI reaching significance by 16 weeks after TBI ($p<0.05$; Fig 6D) with a similar pattern seen for *Cdkn2a*. Analysis of markers of the SASP, fibrosis and *Bcl2* family (measured by qPCR; Fig 6E) and the senescence marker SA-β-Gal (Fig 6F) all had higher means at week 16 post irradiation, but with a high biological variation.

IF staining demonstrated increased P16INK4A protein expression by 16 weeks post-TBI ($p<0.01$; Fig 6G). In line with previous observations in the lung after TBI (*15*), senescence in the kidneys rose modestly by 8 weeks post-TBI, reaching significance by 16 weeks, a finding compatible with ongoing SASP activation driving progressive late senescence distinct from the initial genotoxic insult. Consistent with these findings, TBI drove initiation of the DDR in the diseased kidney, with maximal increases seen in the cortex, mirroring findings in aged kidneys (Fig 6H). Collagen I increased at 16 weeks post-TBI ($p<0.01$; Fig 6I) with a similar pattern seen on PSR staining (Fig 6J).

To test the sensitivity of irradiation induced SCs to senolytic therapy, mice were treated with ABT-263 before kidney harvest at 20 and 25 weeks post-TBI (Fig S3A). *Cdkn1a* (P21CIP1) mRNA was significantly decreased with senolytic treatment as measured by qPCR ($p<0.05$;

Fig S3B). Whilst no change in *Cdkn2a* transcript levels was detected P16INK4A protein abundance also fell post-ABT-263-treatment (Fig S3C-D). *Lmnb1* was found to increase in the post-TBI kidney in ABT-263 treated mice (Fig S3E) at 20 weeks post-TBI. ABT-263 reduced evidence of the DDR in the irradiated kidney, with a reduction in positive γH2A.X positive nuclei in the cortex of treated kidneys ($p<0.05$; Fig S3F). Fibrosis as measured by PSR staining for collagen did not differ between groups, indicating that ABT-263 had no detectable impact on established fibrosis (Fig S3G).

**Irradiation worsens fibrotic responses to subsequent renal injury, which is prevented by ABT-263 pre-treatment**. To dissect the effect of senescence on subsequent injury responses from generic aging effects, we compared post-IRI kidney disease outcomes in young irradiated mice with increased numbers of senescent cells (+/- ABT-263, Fig 7A).

PSR staining for collagen showed that previous TBI increased fibrosis in post-IRI kidney disease, which was prevented with senolytic treatment (Fig S4A-B). qPCR analysis of the profibrotic factors *Col1a1*, *Col3a1*, *Fn1* (Fibronectin 1) and *Acta2* (α-SMA) demonstrated that post-IRI fibrosis/matrix deposition was exacerbated by prior TBI, with ABT263 pretreatment providing protection (Fig S4C-F). IRI induced renal *Cdkn1a* (P21CIP1) and *Cdkn2a* expression in age-matched control mice (in the young range ~30 weeks old), showing that senescence is induced in young kidneys after IRI, in agreement with published reports (*6, 30*). However, these were higher in pre-irradiated mice ($p<0.05$) unless pre-treated by ABT-263 ($p<0.01$) (Figs 7B and S4G). A similar pattern was found in P16INK4A protein abundance (IF; Fig S4H).

SA-β-Galactosidase quantification in diseased kidneys post-IRI confirmed that senescence was further increased by previous TBI and was reversed with ABT-263 (Fig S4I). qPCR showed that SASP markers (*Il6, Tnf*, and *Tgfb1*) also increased in post-IRI kidney disease, were higher with irradiation, and reduced with senolytic treatment (Fig S4J-L). *Bcl2* was also reduced by ABT-263 treatment in irradiated animals (Fig S4M). There were significantly more Lamin B1 positive tubular nuclei in the kidneys of irradiated mice pre-treated with the senolytic before IRI ($p<0.01$; Fig S4N). γH2A.X quantification post-IRI confirmed that DNA damage and DDR were further increased by previous TBI and were reversed with ABT-263, with maximal changes seen in the renal cortex (Fig S4O-P).

Post-IRI kidney disease decreases kidney mass due to destruction of tubules without appropriate repair. By weighing the post-IRI and contralateral kidneys we demonstrated that IRI reduces kidney weight, with prior irradiation causing greater weight loss. ABT-263 pretreatment led to significantly less weight loss reflecting improved tubular regenerative capacity ($p<0.01$; Fig 7C; dashed line represents healthy weight ratio). We also examined ongoing renal damage by analysing chronic KIM-1 expression in the diseased kidney post-IRI. KIM-1 was elevated after irradiation and lowered by ABT-263 administration ($p<0.01$; Fig 7D).

LTL+ tubules were co-stained with Ki67 to measure proliferation (Fig 7E). ABT-263 treatment increased numbers of healthy LTL+ tubules present post-IRI (Fig 7F). Many LTL- cells had Ki67+/DAPI+ nuclei in post-IRI kidney disease representing proliferating interstitial cells (Fig 7E, red arrows). The number of Ki67+ nuclei associated with LTL+ tubules were counted (Fig 7E, yellow arrows). ABT-263 administration significantly increased Ki67+ tubules ($p<0.05$; Fig 7G), indicating that senescence impairs tubular

regeneration after injury, with senolytic treatment restoring regenerative capacity to previously irradiated kidneys. Dual staining with Ki67 and p21CIP1 demonstrated that these two markers were mutually exclusive, confirming that Ki67 did not reflect the amount of senescence (Fig S4Q).

TGF-β1 protein, as measured in injured kidney lysates, was highest after irradiation and was reduced with senolytic treatment ($p<0.05$; Fig 7H), in agreement with reductions observed in transcript expression (Fig S4L) and in aged mice (Fig 4G), indicating that SCs are a major determinant of renal TGF-β1. Due to the effect of TGF-β1 on macrophages post-IRI, we next investigated macrophage numbers and phenotype. F4/80 IHC and *Cd68* qPCR analysis (Fig S5A-C) confirmed an increase in macrophage influx after IRI post-TBI, compared to non-irradiated kidneys. Senolytic treatment reduced CD206+ pro-fibrotic macrophages in the IRI kidney of TBI mice ($p<0.05$; Fig S5D).

Last, we undertook bilateral IRI studies to establish whether senescent cell depletion restored functional regeneration in the young, irradiated kidney (Fig 8A). These studies demonstrated that irradiated mice treated with ABT-263 prior to IRI had improved renal function measured by serum Cystatin C ($p<0.01$ both for d7 and d35; Fig 8B) and reduced numbers of p21CIP1+ senescent cells after injury ($p<0.01$; Fig 8C). This functional protection was accompanied by reduced renal fibrosis by both PSR staining (Fig 8D-E) and Collagen I analysis by IF (Fig 8F-G). Dual staining of P16INK4A with Collagen I and p21CIP1 with Collagen I demonstrated that markers of both arms of the senescence induction pathway correlated with collagen deposition in the immediate surrounding tissue of the kidney (Fig 8H-I).

Of note, age-matched young non-irradiated mice were included in all the groups above as additional controls. In all cases, ABT-263 therapy had no impact on these mice compared to vehicle treatment in any parameter studied (Figs S6A-G), so for simplicity they have otherwise been omitted from the presented data. This finding illustrates that in the absence of increased numbers of pre-injury senescent cells ABT-263 exerts no other protective effect on non-senescent cells such as epithelia, mesenchyme or leukocytes.

The presence of senescent cells impaired structural and functional recovery after injury and promoted fibrosis in both naturally aged and young irradiated mice. Furthermore, pre-injury depletion of senescent cells improved renal structural and functional regenerative capacity.

**Discussion**

Aged patients are known to be at elevated risk of acute kidney injury and subsequent progressive chronic kidney disease (*3*). Several studies have shown correlations between increased senescence within the kidney and progression of CKD, or with adverse outcomes after transplantation (*9, 31-35*). Whether senescent cells themselves directly influence impaired repair and drive fibrosis after subsequent injury remains a key unanswered question. Determining the safety and efficacy of senescent cell depletion prior to renal injury would clarify the contribution of senescent cells to repair and fibrosis and would be of translational importance for aged patients at risk of AKI and CKD.

Whereas aged patients are most susceptible to AKI and CKD, murine models of AKI and CKD are typically undertaken in young healthy animals. In this study, we tested the impact of senescence on renal regenerative capacity by using both naturally aged and young irradiated mice, demonstrating that cellular senescence increased fibrosis and inhibited regeneration following AKI. Pre-treatment with the senolytic ABT-263 reduced senescent cell number, augmented epithelial proliferation and reduced deposition of fibrosis in the aftermath of renal injury in both aged and young irradiated mice, similar to healthy young mice. These findings are consistent with and extend previous interventions with senolytics on the uninjured kidney (*7, 18*). Based on these data and supporting evidence from the literature that senescent epithelial cell growth arrest suppresses regenerative capacity (*36, 37*) we propose that senescent cells in the kidney represent a key determinant of renal regenerative capacity in vivo. These findings mirror those recently reported in other organ systems including the lung and liver (*38, 39*). SASP factor release has been shown to activate myofibroblasts to secrete matrix with TGF-β1, a prime candidate as a known fibroblast activator and mitogen (*40*). In

this study, TGF-β1 decreased after IRI (RNA and protein) with senolytic pretreatment, implicating senescence as a major regulator of TGF-β1 expression and release.

These data support the hypothesis that chronically senescent cells are deleterious to longer term renal homeostasis and function. In the models of aging and injury studied, senescent cell depletion pre-injury improved subsequent renal regenerative capacity and reduced fibrosis. Further studies would be indicated including assessment of long-term pharmacological treatment of senescence on kidney structure and function, and trials of clinically licenced agents capable of suppressing SASP factor release (*41*). Given the reported importance of senescence in acute wound repair it will be important to assess the optimal timing of senescent depletion, as the safety and efficacy of depletion in the aftermath of acute injuries such as renal transplantation and post-surgical AKI remains unknown.

ABT-263 has been found to be selectively toxic to senescent cells via its actions on Bcl2/w/xL (*15*), but prolonged dosing has been complicated by thrombocytopaenia occurring as an on-target effect of Bcl-2 inhibition (*42*). Importantly, the selectivity of ABT-263 for senescent human epithelia in vitro could facilitate its use in carefully selected patients, where the limited duration of dosing required for senolysis minimises bleeding risk. In the work presented here ABT-263 was safe and efficacious in senescent cell depletion and preservation of renal regenerative capacity with no gastrointestinal distress, toxicity or bleeding problems detected. On the basis of the results reported here, approval has been granted for a pre-clinical study to quantify the efficacy and safety of ABT-263 administration to ex-vivo human kidneys that have been rejected for transplantation in man. Should efficacy and safety in human kidneys be similar to the results in experimental animals, further studies should

investigate treating kidneys prior to transplantation, and high-risk patients with CKD prior to surgical procedures with high risks of AKI.

There are several limitations to this study which should be addressed in future research. Whereas two distinct modes of senescent cell generation (irradiation and natural aging) were studied, this does not encompass the full range of senescence-generating stimuli present in human aging and kidney disease. Our study focused on the role of senescent cells present prior to a further renal injury and did not address the therapeutic efficacy of post-injury senescent cell depletion. Finally, our study used ABT-263 as our senolytic agent for all in vivo work, and the efficacy of alterative senolytic drugs with different modes of action remain to be determined in both murine models of disease and in human patients. The findings presented here support further studies using alternative senolytic drugs, timings of administration and modes of senescence induction to establish the breadth of potential benefits for senescent cell depletion.

This work demonstrates cellular senescence to be a key determinant of renal regenerative capacity and a mediator of post-injury fibrosis and function. Furthermore, our data show that senolytic treatment may be efficacious as an intervention in populations with pre-existing SCs including the elderly, those with CKD and previously irradiated patients. With several agents, including ABT-263, entering clinical trials, there is the potential for senolysis to fill an unmet need for those with elevated senescence who are heightened risk of progressive fibrotic renal disease.

## Materials and Methods

*Study Design*

This study addressed the hypothesis that senescent cells present in the aged and young, prematurely senescent kidney negatively impact the ability of the kidney to regenerate from injury, and that their therapeutic depletion would therefore be protective. A series of controlled laboratory experiments were performed to determine the degree of fibrosis present in the kidney after injury with and without treatment with ABT-263 in vivo. All studies were conducted in accordance with ARRIVE guidelines (Animal Research: Reporting of In Vivo Experiments) (*43*). Based on previous work a two-sided two sample test was used to generate group sizes for all studies. All studies were performed at the University of Edinburgh, UK, with data collection performed at pre-specified endpoints unless limited by animal distress as identified by facility staff and/or veterinary surgeons. No available data was excluded from the analysis. Primary and secondary endpoints were pre-specified. Each mouse represented one experimental unit. In all experiments, there was randomised allocation to groups. Drug administration and surgical timing was rigorously rotated across all groups. Tissue was collected by two staff members blinded to the treatment groups, using a coding system for each animal. Semi-blinded staining and image analysis was undertaken with unblinding only being performed after all data acquisition was complete.

*Human biopsies*

After appropriate ethical approval from Tissue Governance at the Royal Infirmary of Edinburgh, sections were obtained from renal biopsy tissue from n=10 renal biopsies, selected to encompass a range of renal function spanning from normal to stage IV chronic kidney disease. Slides were cut and immunohistochemistry performed for P16INK4A and

P21CIP1. Staining was performed in the UKAS (United Kingdom Accreditation Service) certified laboratory of Edinburgh Royal Infirmary stained on Leica Bond III autostainers using Bond Refine detection kits (Peroxidase-DAB detection). Antibodies to P16INK4A were produced by Cintech, supplied by Roche/Ventana and used at 1:1 dilution. Antibodies to P21CIP1 were produced by Leica (code NCL-L-WAF1(P21)) and used at 1:20 dilution. Both underwent high pH antigen retrieval for 20 minutes. Transcriptomic datasets were obtained from published and publicly available resources from 95 renal transcriptomes from eligible studies in Nephroseq (University of Michigan, Ann Arbor, MI) (*16, 17*).

*Cell culture*

Human renal proximal tubular epithelial cells (hRPTEC; ATCC) were maintained in Dulbecco's Modified Eagle Medium (DMEM)-F-12 + Glutamax-1 supplemented with hTERT immortalised RPTEC growth kit (ATCC) and 50mg/ mL Geneticin (Gibco-life Technologies). Cells were grown at 37˚C in 5% $CO_2$. hRPTEC cells were plated at 2 x $10^5$ cells per well of a 6-well plastic culture dish. After overnight culture, these cells were exposed to 10 Gy radiation. Cells were incubated for 7 days with media change every 3-4 days. For senolytic treatment with ABT-263 100,000 PTECs were seeded onto a 12-well plate. The following day, they were exposed to 10Gy Gamma radiation. For ABT-263 treatment, on day 5, 0.1, 1 and 5uM ABT-263 was added to the culture (replenished every 48 hours) until 12 days post-irradiation when the cells were washed with PBS. Cells were analysed on day 14.

Random fields of view within the plate (at x20 magnification) were captured using light microscopy on an Evos microscope. Scaling was performed using a graticule. Lines were drawn around 5 random cells per well, with area calculated using ImageJ (NIH, USA) (*44*).

For each well, multiple random fields of view were captured for analysis and the results averaged prior to cell lysis in trizol for RNA extraction.

*Senescence associated (SA)-β-Galactosidase staining*

Staining was performed as per manufacturer's instructions (Cell Signalling Technology, London, UK). Briefly, samples were fixed using reagents provided before staining (pH 6), in low $CO_2$ incubators. RPTECs were imaged after 3 hours of incubation. For kidney, frozen sections were air dried before staining for 12 hours. Nuclear fast red was used to counterstain slides, before dehydration and mounting. To analyse RPTEC staining, total cells per field were counted and then SA-β-Galactosidase+ cells (blue) were counted, and % SA-β-Galactosidase+ calculated. For kidney sections, fields of view at x10 magnification were captured. % positivity (areas of blue) was calculated over multiple random fields of view using ImageJ imaging software.

*Experimental mice*

All mice were on either a C57BL/6 or a mixed genetic background. All experiments comprised male mice, unless otherwise stated. Ages ranged from 6-8 weeks for young and 18-24 months for old. Mice were bred and maintained at the University of Edinburgh or purchased from Harlan, UK. Paraffin embedded samples of kidney tissue from P16INK4A WT and P16INK4A KO mice were sourced from our collaborators Dr Krimpenfort at the Netherlands Cancer Institute and Professor Melk and Dr Schmitt at Hannover Medical School. All animal work was compliant with IACUC guidelines, conducted in accordance with the UK Government Animals (Scientific Procedures) Act 1986, in conventional barrier unit facilities with conventional bedding, 12:12h light:dark cycle, ambient temperature control and access to food and water ad libitum and was approved by the University of

Edinburgh Ethical Review Committee.

*ABT-263 senolytic treatment*

ABT-263 (Chemgood, VA, USA) was prepared in 10% Ethanol, 30% polyethylene glycol (PEG) 400 and 60% Phosal 50PG. ABT-263 was administered by gavage (50 mg/kg/day) daily for 2 cycles, each of 7 days.

Mice that had undergone TBI were treated with ABT-263 or vehicle at 15 and 18 weeks post-TBI, or at an equivalent age for age matched controls. At week 20, mice underwent unilateral ischaemia-reperfusion injury surgery (IRI) or were culled for tissue analysis. A subset of mice that had undergone TBI were treated with ABT-263 or vehicle at 15, 18 and 35 weeks post-TBI. ABT-263 was administered by gavage (50 mg/kg/day) daily for 3 cycles, each of 7 days. At week 37, mice underwent bilateral IRI for kidney function measurement.

*Ischaemia Reperfusion Injury (IRI)*

IRI surgery was performed as previously described (*45*). Anesthesia was induced with 2% iso-fluorane. Buprenorphine analgesia was administered subcutaneously. A mid-line laparotomy was performed and the left renal pedicle identified and clipped using an atraumatic clamp for 15 min. During the ischemic period, body temperature was maintained using a heating blanket with homeostatic control (Harvard Apparatus) via a rectal temperature probe. After clamp removal, peritoneal closure with 5/0 suture and skin closure with clips was performed prior to subcutaneous administration of 1mL 0.9% saline. The right kidney was uninjured in some surgeries (unilateral IRI) and is referred to as the contralateral kidney. In later experiments, both kidneys were clamped (bilateral IRI). Animals were maintained for 2-5 weeks post-IRI before tissue harvest. Kidneys were weighed at time of sacrifice. Tissue was fixed in methcarn (Methanol 60%, Chloroform 30%, Glacial Acetic

Acid 10%) or snap frozen in liquid nitrogen/dry ice. In later experiments, tissue was also fixed in 4% paraformaldehyde, as this was found to be optimal for p21CIP1 antibody staining allowing us to carry out IHC for this extra marker, which was not possible in earlier experiments.

*Murine irradiation*

Young mice were exposed to a sub-lethal dose (7 Gy) of total body irradiation (TBI) using a closed caesium-137 gamma source. Age-matched control mice were not irradiated but housed in the same facility and conditions. A subset of irradiated mice were culled 8, 16, 20 and 25 weeks after exposure for tissue analysis of radiation-induced renal senescence.

*Immunohistochemistry (IHC)*

Picrosirius red: For picrosirius red (PSR) staining, sections were deparaffinised and rehydrated before treatment in haematoxylin for 8 minutes. After washing, these were stained in picrosirius red for 1 hour, before acidified water washing, dehydration and mounting.

H&E: sections were deparaffinised and rehydrated before staining with haematoxylin and eosin, before acidified water washing, dehydration and mounting.

DAB Staining: Tissue was fixed in methacarn overnight, changed to 70% ethanol and processed. Briefly, paraffin embedded tissue sections (5 μM) were deparaffinised and rehydrated. Antigen unmasking was undertaken (see table S2). Endogenous peroxidase was quenched with 3% $H_2O_2$ (Sigma Aldrich) for 15 minutes, before avidin/biotin (Vector) and protein blocking (DAKO) for 10 minutes each. Slides were then incubated with antibody overnight at 4$^{o}$C. Species-appropriate biotinylated secondary antibodies (1:200) were added and staining developed using the Vector ABC kit and 3,3$'$-diaminobenzidine (DAB).

To investigate the distribution of DNA damage/senescence in young, aged and irradiated kidneys, pre- and post-IRI, γH2A.X IHC was carried out. Images of whole kidneys were collected as .CZI files on the Zeiss AxioScan. This allowed visualisation of full kidney sections using QuPath(*46*). Sections were divided into Inner Medulla, Outer Medulla and Cortex, and areas within these analysed for % γH2A.X positivity.

*Immunofluorescence (IF)*

For IF staining, paraffin embedded tissue sections were deparaffinized and rehydrated. Antigen unmasking was undertaken (see table S2). Slides were incubated with protein block for 30 minutes before addition of the primary antibodies overnight at 4°C. Secondary antibodies are specified in table S2 (1:200, 1:500 or 1:1000 dilution). The slides were mounted with Vectashield with DAPI (Vector).

Kidney sections were visualized and captured using the Zeiss Axioskop 2mot+ or on an Axioscan slidescanner. % area of positivity was calculated in ImageJ or in QuPath (*46*). In light of concerns about the specificity of antibodies to P16INK4A, staining performed in normally aged and post-IRI kidneys from P16INK4A -/- and WT mice confirmed that AHP1488 detected no p19ARF protein in aged or injured kidneys (Fig S7). To measure correlation between SCs and collagen staining, dual IF was carried out for the P21CIP1 or P16INK4A proteins (red fluorescence) and COL I (green fluorescence) on all relevant kidney sections. Images of these kidneys were collected as CZI files on the AxioScan. This allowed visualisation of full kidney sections in the QuPath programme. % positivity for p21CIP1 and P16INK4A proteins (red) and Col I (green) was assessed from 3-7 random fields per kidney (ImageJ macro). These values were collated and analysed together to assess any linear correlation. A scatter plot was generated, a trendline added and, $R^2$ and P values calculated in

Microsoft Excel. For Lamin B1 calculations, total tubular (LTL+) DAPI+ and Lamin B1+ nuclei were counted per field and % Lamin B1+ nuclei per tubule calculated. For *Lotus tetragonolobus* lectin (LTL)/Ki67 dual staining, total LTL+ tubules and LTL+ tubules containing Ki67+ nuclei were counted and % Ki67+ tubules calculated.

*RNA extraction and qPCR*

RNA was extracted from human PTECS or murine kidneys using TRIZOL (Invitrogen, Carlsbad, CA) according to the manufacturer's instructions and reverse transcribed to cDNA (Qiagen Quantitect Reverse Transcription Kit). qPCR was carried out using VWR Perfecta qPCR mastermix with TAQman® gene expression assays on a Roche Lightcycler 480 using standard protocol.

For human RPTEC cells, the TAQman® gene expression assays used were glyceraldehyde 3-phosphate dehydrogenase (Hs02758991_g1 GADPH), hypoxanthine-guanine phosphor-ribosyltransferase (Hs02800695 HPRT1), peptidylprolyl isomerase A (Hs04194521 PPIA), MKI67 (Hs04260396_g1, KI67), Laminb1 (Hs01059210_m1 LMNB1), *Cdkn2a* (Hs00923894_m1 CDKN2A), P21CIP1 (Hs00355782_m1 CDKN1A), Interleukin (Il)-1b (Hs01555410_m1 IL1B), Il6 (Hs00174131_m1 IL6), tumour necrosis factor (Hs00174128_m1 TNF), transforming growth factor (Hs00998133_m1 TGFB1), Cxcl8 (Hs00174103_m1 CXCL8), Matrix metalloproteinase 1 (Hs00899658 MMP1), Bcl (B cell lymphoma)-2 (Hs04986394_s1 BCL2), Bcl-xl (Hs00236329_m1 BCL2L1), Bcl-w (Hs01573809_g1 BCL2L2), prob FOXO4 (Hs00172973 FOXO4). mRNA expression was normalized for GAPDH, HPRT1 and PPIA (average) expression and presented as fold increases over day 7 non-irradiated cells analysed in parallel.

For murine kidneys, the following TAQman® gene expression assays were used: House keeping genes: hypoxanthine-guanine phosphoribosyltransferase (Mm03024075_m1 Hprt), Gapdh (Mm99999915_g Gapdh), Peptidylprolyl Isomerase A (Mm0234230 PPia) Phosphoglycerate kinase 1 (Mm00435617_m1 Pgk1); Senescence and SASP markers: *Cdkn2a* (Mm00494449_m1 Cdkn2a), P21CIP1 (Mm04205640_g1 Cdkn1a), Il-6 (Mm00446190_m1 Il6), Tnf (TNF; Mm00443258_m1 Tnf), transforming growth factor (Tgf; Mm01178820_m1 Tgfb1), Lamin B1 (Mm00521949 Lmnb1) BCL-2 family members: Bcl-2 (Mm0477631 Bcl2), Bcl-xl (Mm00437783 Bcl2l1), Bcl-w (Mm0043054 Bcl2l2); Macrophage marker: CD68 (Mm03047343_m1 Cd68), Fibrosis markers: collagen (col)1a1 (Mm00801666_g1 Col1a1), Col3a1 (Mm01254476_m1 Col3a1), fibronectin (Mm01256744_m1 Fn1), α-smooth muscle actin (Mm00725412_s1 Acta2). mRNA expression was normalized for HPRT or average HK expression in the case of old IRI tissue and presented as fold increases over naïve or age-matched control analysed in parallel.

*ELISAs*

TGF-β1 ELISA: Protein was extracted from whole kidneys using complete RIPA buffer containing protease inhibitors (Santa Cruz). Briefly, kidney tissue was weighed and then placed in 300 µl RIPA buffer with a 5 mm steel ball in a 2 ml eppendorf tube. The tissue was disrupted by high-speed shaking using a tissue lyser (Qiagen). Samples were placed on ice for 10 minutes before centrifugation for 20 minutes at 10,000g at 4°C prior to supernatant collection. Latent TGF-β1 was activated using 1N HCL for 10 minutes, neutralization with 1.2N NaOH/0.5M HEPES, then analysed on a TGF-β1 ELISA (R&D; Duoset ELISA kit) according to the manufacturer's instructions.

Cystatin C ELISA for Kidney Function: Tail vein blood was recovered from mice that had undergone bilateral IRI 7, 14 or 35 days previously in an equal volume of 4% Citrate buffer before centrifugation at 5000g for 5 minutes at 4°C. 2ul of the clear phase was transferred into 250ul PBS -/- with 0.5% BSA. The mouse cystatin C ELISA (R&D; Duoset ELISA kit) was carried out according to the manufacturer's instructions.

*Statistical Analysis*

Data were analysed with Microsoft Excel, Prism software (GraphPad) or R version 4. Multivariable linear regression was performed on R using the finalfit package (1.0.2). All values are expressed as mean values with error bars representing standard deviations. For all in vivo studies n numbers reflect biological replicates. Depending on the results of normality testing groups were compared using unpaired Student's *t*-test, Mann-Whitney or one/two-way ANOVA (Tukey post-hoc test) were used for analysis. P-values $< 0.05$ denote statistical significance, *$p<0.05$, **$p<0.01$, ***$p<0.005$, ****$p<0.001$.

**List of supplementary materials**

**Figure S1. Expression of selected cyclin dependent kinase inhibitors, SASP factors, fibrotic and Bcl-2 family transcripts detected on microarray analysis in CKD patients and healthy controls, along with adjusted q-values and fold-change (adapted from Nakagawa et al(*17*))**

**Figure S2. Pre treatment with ABT-263 in aged murine kidneys results in a reduction of fibrosis, DNA damage and macrophages, and favours a reduction of SC/SASP/BCL2 family members and a preservation of LTL+ tubules after injury**.

**Figure S3. ABT-263 treatment reduces expression of *Cdkn1a* and *Cdkn2a* transcripts, reduces cortical γH2A.X expression and increases Lamin B1 in the murine kidney.**

**Figure S4. Irradiation-induced epithelial senescence promotes fibrosis and senescence in murine kidneys with ABT-263 treatment protective.**

**Figure S5**: **Treatment with ABT-263 alters qPCR and protein markers of macrophage infiltration within the murine kidney.**

**Figure S6: The efficacy of pre-treatment with ABT-263 is lost in young mice with low quantities of pre-IRI senescent cells.**

**Figure S7: BioRad Antibody AHP1488 anti-*Cdkn2a* detects P16INK4A but not p19ARF protein expression in aged and fibrotic murine kidneys.**

**Table S1. Multivariate analysis of CDKN1A and CDKN2A and their effect on estimated glomerular filtration rate (egfr) in humans.**

**Table S2. Primary and secondary antibodies used for IHC and IF.**

**Data file S1. Raw data for all figures.**

## References


1. G. B. D. C. K. D. Collaboration, Global, regional, and national burden of chronic kidney disease, 1990-2017: a systematic analysis for the Global Burden of Disease Study 2017. *Lancet* **395**, 709-733 (2020); published online EpubFeb 29 (10.1016/S0140-6736(20)30045-3).
2. J. Coresh, E. Selvin, L. A. Stevens, J. Manzi, J. W. Kusek, P. Eggers, F. Van Lente, A. S. Levey, Prevalence of chronic kidney disease in the United States. *JAMA* **298**, 2038-2047 (2007); published online EpubNov 07 (10.1001/jama.298.17.2038).
3. A. Ishani, J. L. Xue, J. Himmelfarb, P. W. Eggers, P. L. Kimmel, B. A. Molitoris, A. J. Collins, Acute kidney injury increases risk of ESRD among elderly. *J Am Soc Nephrol* **20**, 223-228 (2009); published online EpubJan (10.1681/ASN.2007080837).
4. B. Berkenkamp, N. Susnik, A. Baisantry, I. Kuznetsova, C. Jacobi, I. Sorensen-Zender, V. Broecker, H. Haller, A. Melk, R. Schmitt, In vivo and in vitro analysis of age-associated changes and somatic cellular senescence in renal epithelial cells. *PLoS One* **9**, e88071 (2014)10.1371/journal.pone.0088071).
5. J. Liu, J. R. Yang, Y. N. He, G. Y. Cai, J. G. Zhang, L. R. Lin, J. Zhan, J. H. Zhang, H. S. Xiao, Accelerated senescence of renal tubular epithelial cells is associated with disease progression of patients with immunoglobulin A (IgA) nephropathy. *Translational research : the journal of laboratory and clinical medicine* **159**, 454-463 (2012); published online EpubJun (10.1016/j.trsl.2011.11.008).
6. C. Luo, S. Zhou, Z. Zhou, Y. Liu, L. Yang, J. Liu, Y. Zhang, H. Li, Y. Liu, F. F. Hou, L. Zhou, Wnt9a Promotes Renal Fibrosis by Accelerating Cellular Senescence in Tubular Epithelial Cells. *J Am Soc Nephrol* **29**, 1238-1256 (2018); published online EpubApr (10.1681/ASN.2017050574).
7. D. J. Baker, B. G. Childs, M. Durik, M. E. Wijers, C. J. Sieben, J. Zhong, R. A. Saltness, K. B. Jeganathan, G. C. Verzosa, A. Pezeshki, K. Khazaie, J. D. Miller, J. M. van Deursen, Naturally occurring p16(Ink4a)-positive cells shorten healthy lifespan. *Nature* **530**, 184-189 (2016); published online EpubFeb 11 (10.1038/nature16932).
8. M. P. Baar, R. M. Brandt, D. A. Putavet, J. D. Klein, K. W. Derks, B. R. Bourgeois, S. Stryeck, Y. Rijksen, H. van Willigenburg, D. A. Feijtel, I. van der Pluijm, J. Essers, W. A. van Cappellen, I. W. F. van, A. B. Houtsmuller, J. Pothof, R. W. de Bruin, T. Madl, J. H. Hoeijmakers, J. Campisi, P. L. de Keizer, Targeted Apoptosis of Senescent Cells Restores Tissue Homeostasis in Response to Chemotoxicity and Aging. *Cell* **169**, 132-147 e116 (2017); published online EpubMar 23 (10.1016/j.cell.2017.02.031).
9. A. Melk, P. F. Halloran, Cell senescence and its implications for nephrology. *J Am Soc Nephrol* **12**, 385-393 (2001); published online EpubFeb (
10. A. Melk, W. Kittikowit, I. Sandhu, K. M. Halloran, P. Grimm, B. M. Schmidt, P. F. Halloran, Cell senescence in rat kidneys in vivo increases with growth and age despite lack of telomere shortening. *Kidney Int* **63**, 2134-2143 (2003); published online EpubJun (10.1046/j.1523-1755.2003.00032.x).
11. A. Melk, E. S. Mansfield, S. C. Hsieh, T. Hernandez-Boussard, P. Grimm, D. C. Rayner, P. F. Halloran, M. M. Sarwal, Transcriptional analysis of the molecular basis of human kidney aging using cDNA microarray profiling. *Kidney Int* **68**, 2667-2679 (2005); published online EpubDec (KID738 [pii]
10.1111/j.1523-1755.2005.00738.x).

12. A. Melk, B. M. Schmidt, A. Vongwiwatana, D. C. Rayner, P. F. Halloran, Increased expression of senescence-associated cell cycle inhibitor P16INK4a in deteriorating renal transplants and diseased native kidney. *American journal of transplantation : official journal of the American Society of Transplantation and the American Society of Transplant Surgeons* **5**, 1375-1382 (2005); published online EpubJun (AJT [pii]
10.1111/j.1600-6143.2005.00846.x).
13. B. Zhou, Y. Wan, R. Chen, C. Zhang, X. Li, F. Meng, S. Glaser, N. Wu, T. Zhou, S. Li, H. Francis, G. Alpini, P. Zou, The emerging role of cellular senescence in renal diseases. *J Cell Mol Med* **24**, 2087-2097 (2020); published online EpubFeb (10.1111/jcmm.14952).
14. M. Y. Lee, Y. Wang, P. M. Vanhoutte, Senescence of cultured porcine coronary arterial endothelial cells is associated with accelerated oxidative stress and activation of NFkB. *Journal of vascular research* **47**, 287-298 (2010)10.1159/000265563).
15. J. Chang, Y. Wang, L. Shao, R. M. Laberge, M. Demaria, J. Campisi, K. Janakiraman, N. E. Sharpless, S. Ding, W. Feng, Y. Luo, X. Wang, N. Aykin-Burns, K. Krager, U. Ponnappan, M. Hauer-Jensen, A. Meng, D. Zhou, Clearance of senescent cells by ABT263 rejuvenates aged hematopoietic stem cells in mice. *Nat Med* **22**, 78-83 (2016); published online EpubJan (10.1038/nm.4010).
16. W. Ju, V. Nair, S. Smith, L. Zhu, K. Shedden, P. X. K. Song, L. H. Mariani, F. H. Eichinger, C. C. Berthier, A. Randolph, J. Y. Lai, Y. Zhou, J. J. Hawkins, M. Bitzer, M. G. Sampson, M. Thier, C. Solier, G. C. Duran-Pacheco, G. Duchateau-Nguyen, L. Essioux, B. Schott, I. Formentini, M. C. Magnone, M. Bobadilla, C. D. Cohen, S. M. Bagnasco, L. Barisoni, J. Lv, H. Zhang, H. Y. Wang, F. C. Brosius, C. A. Gadegbeku, M. Kretzler, C. P. N. Ercb, P. K.-I. Consortium, Tissue transcriptome-driven identification of epidermal growth factor as a chronic kidney disease biomarker. *Science translational medicine* **7**, 316ra193 (2015); published online EpubDec 2 (10.1126/scitranslmed.aac7071).
17. S. Nakagawa, K. Nishihara, H. Miyata, H. Shinke, E. Tomita, M. Kajiwara, T. Matsubara, N. Iehara, Y. Igarashi, H. Yamada, A. Fukatsu, M. Yanagita, K. Matsubara, S. Masuda, Molecular Markers of Tubulointerstitial Fibrosis and Tubular Cell Damage in Patients with Chronic Kidney Disease. *PLoS One* **10**, e0136994 (2015)10.1371/journal.pone.0136994).
18. M. P. Baar, R. M. C. Brandt, D. A. Putavet, J. D. D. Klein, K. W. J. Derks, B. R. M. Bourgeois, S. Stryeck, Y. Rijksen, H. van Willigenburg, D. A. Feijtel, I. van der Pluijm, J. Essers, W. A. van Cappellen, I. W. F. van, A. B. Houtsmuller, J. Pothof, R. W. F. de Bruin, T. Madl, J. H. J. Hoeijmakers, J. Campisi, P. L. J. de Keizer, Targeted Apoptosis of Senescent Cells Restores Tissue Homeostasis in Response to Chemotoxicity and Aging. *Cell* **169**, 132-147 e116 (2017); published online EpubMar 23 (10.1016/j.cell.2017.02.031).
19. M. A. Venkatachalam, D. B. Bernard, J. F. Donohoe, N. G. Levinsky, Ischemic damage and repair in the rat proximal tubule: differences among the S1, S2, and S3 segments. *Kidney Int* **14**, 31-49 (1978); published online EpubJul (10.1038/ki.1978.87).
20. B. D. Humphreys, S. Czerniak, D. P. DiRocco, W. Hasnain, R. Cheema, J. V. Bonventre, Repair of injured proximal tubule does not involve specialized progenitors. *Proc Natl Acad Sci U S A* **108**, 9226-9231 (2011); published online EpubMay 31 (1100629108 [pii]

10.1073/pnas.1100629108).
21. W. K. Han, V. Bailly, R. Abichandani, R. Thadhani, J. V. Bonventre, Kidney Injury Molecule-1 (KIM-1): a novel biomarker for human renal proximal tubule injury. *Kidney Int* **62**, 237-244 (2002); published online EpubJul (10.1046/j.1523-1755.2002.00433.x).
22. V. S. Sabbisetti, S. S. Waikar, D. J. Antoine, A. Smiles, C. Wang, A. Ravisankar, K. Ito, S. Sharma, S. Ramadesikan, M. Lee, R. Briskin, P. L. De Jager, T. T. Ngo, M. Radlinski, J. W. Dear, K. B. Park, R. Betensky, A. S. Krolewski, J. V. Bonventre, Blood kidney injury molecule-1 is a biomarker of acute and chronic kidney injury and predicts progression to ESRD in type I diabetes. *J Am Soc Nephrol* **25**, 2177-2186 (2014); published online EpubOct (10.1681/ASN.2013070758).
23. T. Kusaba, M. Lalli, R. Kramann, A. Kobayashi, B. D. Humphreys, Differentiated kidney epithelial cells repair injured proximal tubule. *Proc Natl Acad Sci U S A* **111**, 1527-1532 (2014); published online EpubJan 28 (10.1073/pnas.1310653110).
24. K. R. Spurgeon, D. L. Donohoe, D. P. Basile, Transforming growth factor-beta in acute renal failure: receptor expression, effects on proliferation, cellularity, and vascularization after recovery from injury. *Am J Physiol Renal Physiol* **288**, F568-577 (2005); published online EpubMar (00330.2004 [pii]
10.1152/ajprenal.00330.2004).
25. L. Yang, T. Y. Besschetnova, C. R. Brooks, J. V. Shah, J. V. Bonventre, Epithelial cell cycle arrest in G2/M mediates kidney fibrosis after injury. *Nature medicine* **16**, 535-543, 531p following 143 (2010); published online EpubMay (nm.2144 [pii]
10.1038/nm.2144).
26. S. Chung, J. M. Overstreet, Y. Li, Y. Wang, A. Niu, S. Wang, X. Fan, K. Sasaki, G. N. Jin, S. N. Khodo, L. Gewin, M. Z. Zhang, R. C. Harris, TGF-beta promotes fibrosis after severe acute kidney injury by enhancing renal macrophage infiltration. *JCI Insight* **3**, (2018); published online EpubNov 2 (10.1172/jci.insight.123563).
27. G. Ding, N. Franki, A. A. Kapasi, K. Reddy, N. Gibbons, P. C. Singhal, Tubular cell senescence and expression of TGF-beta1 and p21(WAF1/CIP1) in tubulointerstitial fibrosis of aging rats. *Experimental and molecular pathology* **70**, 43-53 (2001); published online EpubFeb (10.1006/exmp.2000.2346
S0014-4800(00)92346-3 [pii]).
28. J. C. Acosta, A. Banito, T. Wuestefeld, A. Georgilis, P. Janich, J. P. Morton, D. Athineos, T. W. Kang, F. Lasitschka, M. Andrulis, G. Pascual, K. J. Morris, S. Khan, H. Jin, G. Dharmalingam, A. P. Snijders, T. Carroll, D. Capper, C. Pritchard, G. J. Inman, T. Longerich, O. J. Sansom, S. A. Benitah, L. Zender, J. Gil, A complex secretory program orchestrated by the inflammasome controls paracrine senescence. *Nature cell biology* **15**, 978-990 (2013); published online EpubAug (10.1038/ncb2784).
29. M. G. Kim, S. C. Kim, Y. S. Ko, H. Y. Lee, S. K. Jo, W. Cho, The Role of M2 Macrophages in the Progression of Chronic Kidney Disease following Acute Kidney Injury. *PLoS One* **10**, e0143961 (2015)10.1371/journal.pone.0143961).
30. L. Kailong, X. Du, H. Yani, Z. Lin, Y. Jvrong, S. Ruihua, C. Lin, P53-Rb signaling pathway is involved in tubular cell senescence in renal ischemia/reperfusion injury. *Biocell* **31**, 213-223 (2007); published online EpubAug (
31. A. Melk, V. Ramassar, L. M. Helms, R. Moore, D. Rayner, K. Solez, P. F. Halloran, Telomere shortening in kidneys with age. *J Am Soc Nephrol* **11**, 444-453 (2000); published online EpubMar (

32. A. Vongwiwatana, A. Tasanarong, D. C. Rayner, A. Melk, P. F. Halloran, Epithelial to mesenchymal transition during late deterioration of human kidney transplants: the role of tubular cells in fibrogenesis. *American journal of transplantation : official journal of the American Society of Transplantation and the American Society of Transplant Surgeons* **5**, 1367-1374 (2005); published online EpubJun (AJT843 [pii]
10.1111/j.1600-6143.2005.00843.x).
33. A. Melk, B. M. Schmidt, H. Braun, A. Vongwiwatana, J. Urmson, L. F. Zhu, D. Rayner, P. F. Halloran, Effects of donor age and cell senescence on kidney allograft survival. *American journal of transplantation : official journal of the American Society of Transplantation and the American Society of Transplant Surgeons* **9**, 114-123 (2009); published online EpubJan (10.1111/j.1600-6143.2008.02500.x).
34. H. Braun, B. M. Schmidt, M. Raiss, A. Baisantry, D. Mircea-Constantin, S. Wang, M. L. Gross, M. Serrano, R. Schmitt, A. Melk, Cellular Senescence Limits Regenerative Capacity and Allograft Survival. *J Am Soc Nephrol*, (2012); published online EpubJul 12 (ASN.2011100967 [pii]
10.1681/ASN.2011100967).
35. M. H. Docherty, E. D. O'Sullivan, J. V. Bonventre, D. A. Ferenbach, Cellular Senescence in the Kidney. *J Am Soc Nephrol* **30**, 726-736 (2019); published online EpubMay (10.1681/ASN.2018121251).
36. D. Munoz-Espin, M. Serrano, Cellular senescence: from physiology to pathology. *Nature reviews. Molecular cell biology* **15**, 482-496 (2014); published online EpubJul (10.1038/nrm3823).
37. L. Hayflick, P. S. Moorhead, The serial cultivation of human diploid cell strains. *Experimental cell research* **25**, 585-621 (1961); published online EpubDec (
38. M. J. Schafer, T. A. White, K. Iijima, A. J. Haak, G. Ligresti, E. J. Atkinson, A. L. Oberg, J. Birch, H. Salmonowicz, Y. Zhu, D. L. Mazula, R. W. Brooks, H. Fuhrmann-Stroissnigg, T. Pirtskhalava, Y. S. Prakash, T. Tchkonia, P. D. Robbins, M. C. Aubry, J. F. Passos, J. L. Kirkland, D. J. Tschumperlin, H. Kita, N. K. LeBrasseur, Cellular senescence mediates fibrotic pulmonary disease. *Nature communications* **8**, 14532 (2017); published online EpubFeb 23 (10.1038/ncomms14532).
39. S. Ferreira-Gonzalez, W. Y. Lu, A. Raven, B. Dwyer, T. Y. Man, E. O'Duibhir, P. J. S. Lewis, L. Campana, T. J. Kendall, T. G. Bird, N. Tarrats, J. C. Acosta, L. Boulter, S. J. Forbes, Paracrine cellular senescence exacerbates biliary injury and impairs regeneration. *Nat Commun* **9**, 1020 (2018); published online EpubMar 9 (10.1038/s41467-018-03299-5).
40. X. M. Meng, D. J. Nikolic-Paterson, H. Y. Lan, TGF-beta: the master regulator of fibrosis. *Nat Rev Nephrol* **12**, 325-338 (2016); published online EpubJun (10.1038/nrneph.2016.48).
41. O. Moiseeva, X. Deschenes-Simard, E. St-Germain, S. Igelmann, G. Huot, A. E. Cadar, V. Bourdeau, M. N. Pollak, G. Ferbeyre, Metformin inhibits the senescence-associated secretory phenotype by interfering with IKK/NF-kappaB activation. *Aging Cell* **12**, 489-498 (2013); published online EpubJun (10.1111/acel.12075).
42. B. T. Kile, The role of apoptosis in megakaryocytes and platelets. *British journal of haematology* **165**, 217-226 (2014); published online EpubApr (10.1111/bjh.12757).
43. C. Kilkenny, W. J. Browne, I. C. Cuthill, M. Emerson, D. G. Altman, Improving bioscience research reporting: the ARRIVE guidelines for reporting animal research.

*PLoS biology* **8**, e1000412 (2010); published online EpubJun 29 (10.1371/journal.pbio.1000412).
44. C. A. Schneider, W. S. Rasband, K. W. Eliceiri, NIH Image to ImageJ: 25 years of image analysis. *Nature methods* **9**, 671-675 (2012); published online EpubJul (10.1038/nmeth.2089).
45. D. A. Ferenbach, N. C. Nkejabega, J. McKay, A. K. Choudhary, M. A. Vernon, M. F. Beesley, S. Clay, B. C. Conway, L. P. Marson, D. C. Kluth, J. Hughes, The induction of macrophage hemeoxygenase-1 is protective during acute kidney injury in aging mice. *Kidney Int* **79**, 966-976 (2011); published online EpubMay (ki2010535 [pii]
10.1038/ki.2010.535).
46. P. Bankhead, M. B. Loughrey, J. A. Fernandez, Y. Dombrowski, D. G. McArt, P. D. Dunne, S. McQuaid, R. T. Gray, L. J. Murray, H. G. Coleman, J. A. James, M. Salto-Tellez, P. W. Hamilton, QuPath: Open source software for digital pathology image analysis. *Sci Rep* **7**, 16878 (2017); published online EpubDec 4 (10.1038/s41598-017-17204-5).

**Acknowledgements:**

Shared University Research Facilities, Queen's Medical Research Institute, Edinburgh, UK.

Histopathology Laboratory, Royal Infirmary of Edinburgh, Edinburgh, UK.

Nephroseq (https://www.nephroseq.org/resource/login.html) (December 2019, University of Michigan, Ann Arbor, MI).

**Funding**: This work was funded by Project Grant RP_036_20160304 from Kidney Research UK and Intermediate Clinical Fellowship 100171/Z/12/Z from the Wellcome Trust to DAF. SN was supported by a Wellcome Trust Four-Year Ph.D. Program in Tissue Repair [Grant 108906/Z/15/Z].

**Author contributions:**

KJM carried out the experimental design, carried out in vivo experiments, collected the data, performed the analysis, wrote and revised the paper. EDO assisted with data collection and analysis for various figures but in particular Figure 1. They also reviewed the paper. DH assisted with collection of data for Figure 2. DB assisted with collection of the data for Figure 2. MD assisted with collection of the data of IF of p21CIP1 for figures. SAN assisted with

collection of the data for various qPCRs. PJK provided reagents and reviewed the paper. AM provided reagents and reviewed the paper. RS provided reagents and reviewed the paper. SF-G provided reagents and reviewed the paper.

SJF provided supervision and reviewed the paper. JH conceived and designed the analysis, provided supervision and reviewed the paper. DAF conceived and designed the analysis, provided supervision, performed the analysis, assisted with writing and revision of the paper.

**Competing interests**.

All authors declare no competing interests.

**Data and materials availability.**

All data associated with this study are present in the paper or supplementary materials.

**Figure Captions**:

**Figure 1. Markers of cellular senescence increase at transcript and protein abundance in human renal disease.** Datasets published on Nephroseq were examined for human *CDKN1A* and *CDKN2A* transcript expression, and in-house human biopsy samples were stained for P16INKA and P21CIP1 protein expression (**A**). Analysis of two published transcriptomic datasets show that both *CDKN1A* and *CDKN2A* rise in kidneys with chronic kidney disease. Fig 1B: n=48 patients with CKD, n=5 normal controls (*17*) (**B**). In a separate cohort, *CDKN1A* and *CDKN2A* both increase in the kidney with increasing age, n=42, (*16*) (**C**). *CDKN1A* alone correlated with advancing renal impairment, n-42, (*16*) (**D**). Staining performed in a UKAS-certified histology facility demonstrated P16INK4A and P21CIP1 protein expression in patients with CKD (n=10). Sample images are shown from normal

kidneys, early CKD, young patients with radiation nephropathy and from older patients with CKD (**F**; scale bar = 10μm). Expression patterns differed between P21CIP1 and P16INK4A with P21CIP1 expressed predominantly in tubular epithelial nuclei, here shown in a patient with advanced renal fibrosis (**G**). ns=non-significant, **P*<0.05 by unpaired t-test.

**Figure 2. Senescent human tubular epithelial cells demonstrate selective sensitivity to ABT-263 in vitro.** Senescence was induced in human proximal tubular epithelial cells via 10Gy γ-irradiation (**A**). Irradiation resulted in reduced cell number per field (**B**) and increased average cell size (**C**). qPCR analysis of markers of senescence, SASP factors and BCL-2 family members including *MKI67*, *LMNB1*, *CDKN2A*, *CDKN1A*, *TNF*, *IL1B*, *TGFB1*, *BCL2*, *BCL2L1* and *BCL2L2* in irradiated cells (**D**). SA-β-galactosidase (SA-β-Gal) staining in irradiated cells (**E**, scale bar represents 100 μM). RPTECs (control and irradiated) were treated with ABT-263 at various concentrations (0.1, 1 and 5 μMol), and cells per field counted and analysed compared to vehicle controls (**F**). Representative micrographs are shown in lower panel (40 μM scale bar). **P*<0.05, ***P*<0.01. ****P*<0.005, *****P*<0.001. n=4/group. Unpaired *t*-tests used for experimental comparisons in all groups except F : 2-way ANOVA.

**Figure 3. Aged murine kidneys display more senescence, DDR and fibrosis than young kidneys and are more susceptible to post-IRI fibrosis.** Experimental schema of sample collections from young and old mice (**A**). Whole kidney qPCR on samples from young (6-10 weeks) and old mice (>18 months) measuring senescence and SASP markers (**B**). Markers of tissue fibrosis and senescence associated DNA damage were quantified using IF for Collagen I (**C**), PSR (**D**) and γH2A.X IHC (**E**). Representative micrographs are shown in right panels (scale bar represents 50 μM). The % of Lamin $B1^{+}$ (red) nuclei (DAPI; blue) in kidney

tubules (LTL: green) of young vs old kidneys (**F**, n=3-4 group). Representative micrographs are shown in right panels (scale bar represents 20 μM). Old vs young IRI kidneys analysed for collagen deposition (PSR) (**G-H**, comparisons made using one-way ANOVA test with Tukey post-test used). Representative micrographs are shown in right panel (scale bar represents 100 μM). Quantitative PCR of *Cdkn1a* in IRI kidneys from old and young mice compared to naïve kidneys illustrates marked upregulation in both IRI groups (**I**). All groups are n=4-8 with unpaired *t*-tests used for experimental comparisons unless otherwise stated. *$\underline{P}$<0.05, **$P$<0.01. ***$P$<0.005.

**Figure 4. ABT-263 treatment reduces fibrosis and increases the regenerative capacity of aged murine kidneys post-IRI**. Diagram detailing ABT-263 treatment regime and unilateral IRI surgery in old female mice (**A**). qPCR analysis of *Cdkn1a* expression in vehicle and ABT-263-treated mice (**B**; red line=expression in old age-matched control tissue). The weight ratios of IRI/CLK kidneys were also calculated in ABT-263-treated and vehicle-treated mice (**C**; dashed line represents left/right (l/r) kidney ratio in healthy animal). Kidney injury molecule 1 (Kim1/Havcr1) IF analysis of post-IRI kidneys +/- ABT-263 (**D**; representative micrographs are shown; scale bar represents 50 μM). Kidney sections were co-stained for proximal tubule marker LTL (green) and the proliferation marker Ki67 (red). Representative micrograph (**E**) shows the Ki67+ nuclei in LTL+ tubules (white arrows; scale bar represents 50 μM). The % LTL+ tubules positive for Ki67 was calculated in both groups (**F**) TGF-β protein abundance was measured in whole IRI kidney lysates by ELISA (**G**, n=4-5/group).

**Figure 5. ABT-263 treatment improves kidney function in the bilateral IRI model of renal injury.** Diagram detailing ABT-263 treatment regime and bilateral IRI surgery in old

female mice (**A**). Serum Cystatin C is shown at days 7 and 14 post IRI in ABT263 treated mice (**B**; n=7-8/group, Mann-Whitney test). ABT-263 treatment effect on p21CIP1$^{+}$ senescent cells in baseline kidneys (**C**, Mann-Whitney test). PSR staining after IRI to evaluate fibrosis in ABT-263 treated animals (**D**, Mann-Whitney test, n=4-7/group, **E**; representative micrographs are shown; 50 μM scale bar). Collagen I staining by IF after IRI in ABT-263 treated animals compared to controls (**F**, p Mann-Whitney test, n=4-7/group, **G**; representative micrographs are shown; 50 μM scale bar). All n=4-6 per group unless stated, unpaired *t*-tests used for all comparisons unless stated. **P*<0.05, ***P*<0.01.

**Figure 6. Total body irradiation (TBI) drives senescence and fibrosis in young murine kidneys.** Diagram detailing irradiation of mice and analysis of kidneys 8 and 16 weeks post-irradiation (**A**). IHC and whole kidney imaging was used to identify areas of γH2A.X induction (**B, C**). qPCR analysis of whole kidneys for *Cdkn1a* (P21CIP1) and *Cdkn2a* after irradiation (**D**, n=3/6/7 for age matched control (AMC) vs 8 weeks vs 16 weeks post-irradiation, comparisons by one-way ANOVA test with Tukey post-test). qPCR whole kidney for various SASP and BCl-2 family members was carried out (**E**). SA-B-Gal staining and analysis of kidney sections after irradiation (**F**). P16INK4A IF on irradiated kidneys at 8 and 16 weeks post injury (**G**; representative micrographs are shown; 100 μM scale bar). γH2A.X staining of the irradiated kidneys to evaluate DNA damage (**H**; representative micrographs; scale bar represents 50 μM). Collagen I IF of irradiated kidneys at 8 and 16 weeks after irradiation (**I**; representative micrographs are shown; scale bar represents 100 μM,). A similar pattern of PSR staining was seen in naïve and post-irradiated kidneys (**J**). For panels E-F, n=6-8, comparisons by one-way ANOVA test with Tukey post-test. Unpaired t-tests used for all comparisons unless otherwise stated. **P*<0.05, ***P*<0.01. ****P*<0.005.

**Figure 7. Irradiation-induced epithelial senescence impairs post injury renal regeneration and promotes fibrosis in murine kidneys, with ABT-263 pre-treatment providing protection.** Diagram detailing ABT-263 treatment regime and unilateral IRI surgery in irradiated mice (**A**). Whole kidney qPCR for *Cdkn1a* in pre-irradiated kidneys + IRI, compared to IRI alone (**B**), ABT-263 treatment effects on post-ischaemic kidney weight (**C**; dashed line represents l/r kidney ratio in healthy animal) and tubular injury market KIM1 by IHC (**D**). Dual IF staining was performed for Ki67 and the tubular marker LTL (**E,** yellow arrow=$Ki67^{+}LTL^{+}$; red arrow=$Ki67^{+}LTL^{-}$). Quantification of LTL+ tubules (**F**), tubular proliferative capacity (**G**) and renal TGFβ1 protein (**H**).

**Figure 8. Depletion of irradiation-induced senescent cells improves kidney function after subsequent bilateral IRI.** Diagram detailing ABT-263 treatment regime and bilateral IRI surgery in irradiated mice (**A**). Serum Cystatin C concentrations at days 7 and 35 post IRI in ABT263 treated mice (**B**). ABT-263 treatment effects on p21CIP1+ senescent cells in pre-IRI and post-IRI kidneys (**C**). PSR staining after IRI shows effects on fibrosis in ABT-263 treated animals (**D-E**; representative micrographs are shown; 100 μM scale bar, D). Collagen I staining by IF after IRI shows effects on fibrosis in ABT-263 treated animals (**F-G**; representative micrographs are shown; 50 μM scale bar, F). Dual IF staining (P16INK4A red and collagen I; green) was carried out in irradiated IRI kidneys and age matched controls, and regression analysis undertaken to determine correlation between areas of positivity of both proteins (**H**). Further dual IF staining (P21CIP1; red and collagen; green) was carried out in irradiated IRI kidneys and age-matched controls, and regression analysis undertaken to determine correlation between areas of positivity of both proteins (**I**). Key: IRI= ischemia reperfusion injury, Irrad= total body irradiation. n=4-8 per group. Unless otherwise stated comparisons made by unpaired *t*-test. **P*<0.05, ***P*<0.01. ****P*<0.005, *****P*<0.001.

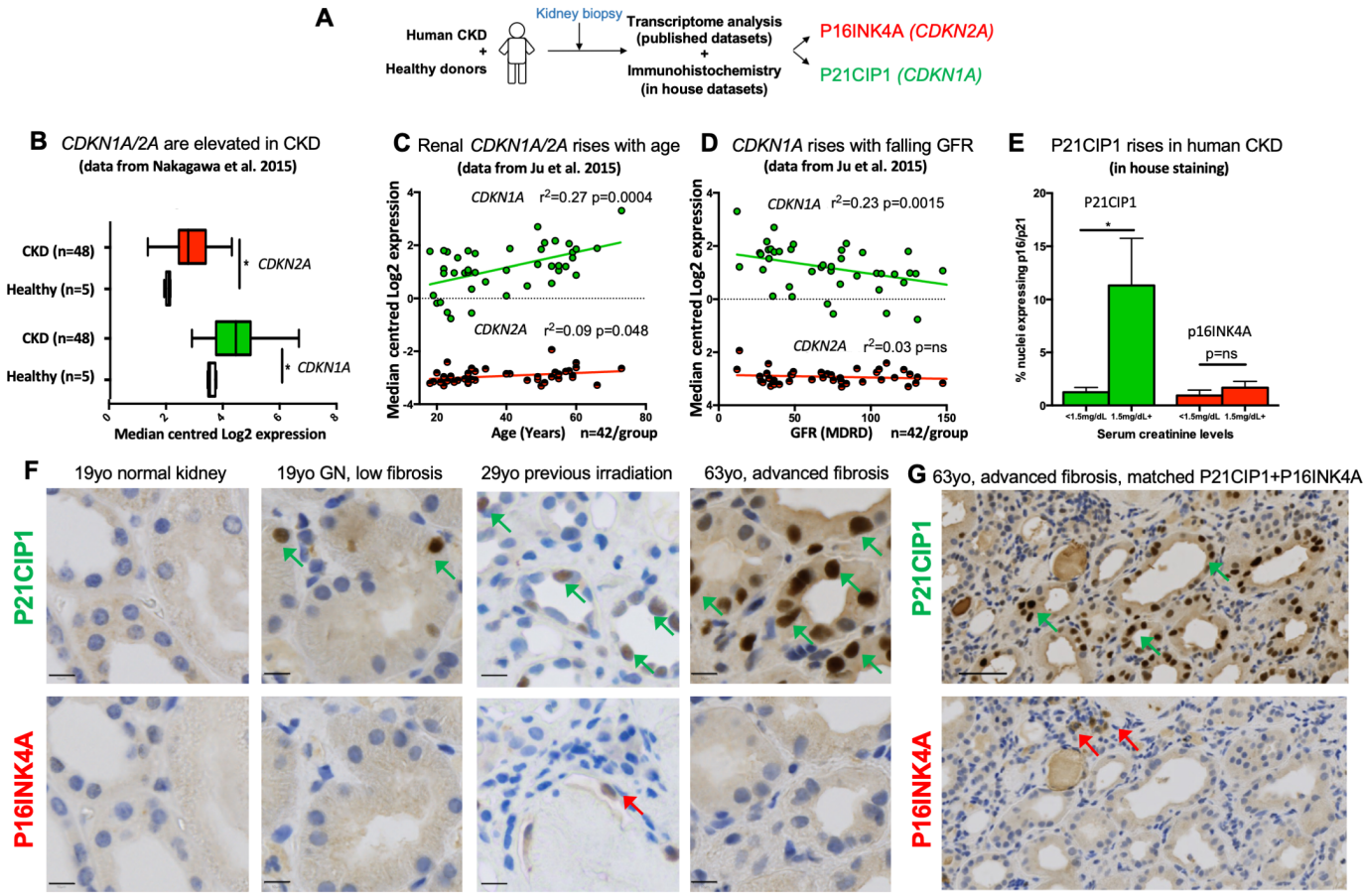
A
Human CKD
+
Healthy donors
Kidney biopsy
Transcriptome analysis
(published datasets)
+
Immunohistochemistry
(in house datasets)
P16INK4A (CDKN2A)
P21CIP1 (CDKN1A)
B CDKN1A/2A are elevated in CKD
(data from Nakagawa et al. 2015)
CKD (n=48)
Healthy (n=5)
* CDKN2A
CKD (n=48)
Healthy (n=5)
* CDKN1A
Median centred Log2 expression
C Renal CDKN1A/2A rises with age
(data from Ju et al. 2015)
Median centred Log2 expression
CDKN1A r2=0.27 p=0.0004
CDKN2A r2=0.09 p=0.048
Age (Years) n=42/group
D CDKN1A rises with falling GFR
(data from Ju et al. 2015)
Median centred Log2 expression
CDKN1A r2=0.23 p=0.0015
CDKN2A r2=0.03 p=ns
GFR (MDRD) n=42/group
E P21CIP1 rises in human CKD
(in house staining)
% nuclei expressing p16/p21
P21CIP1
*
p16INK4A
p=ns
<1.5mg/dL 1.5mg/dL+ <1.5mg/dL 1.5mg/dL+
Serum creatinine levels
F
19yo normal kidney
19yo GN, low fibrosis
29yo previous irradiation
63yo, advanced fibrosis
P21CIP1
P16INK4A
G 63yo, advanced fibrosis, matched P21CIP1+P16INK4A
P21CIP1
P16INK4A

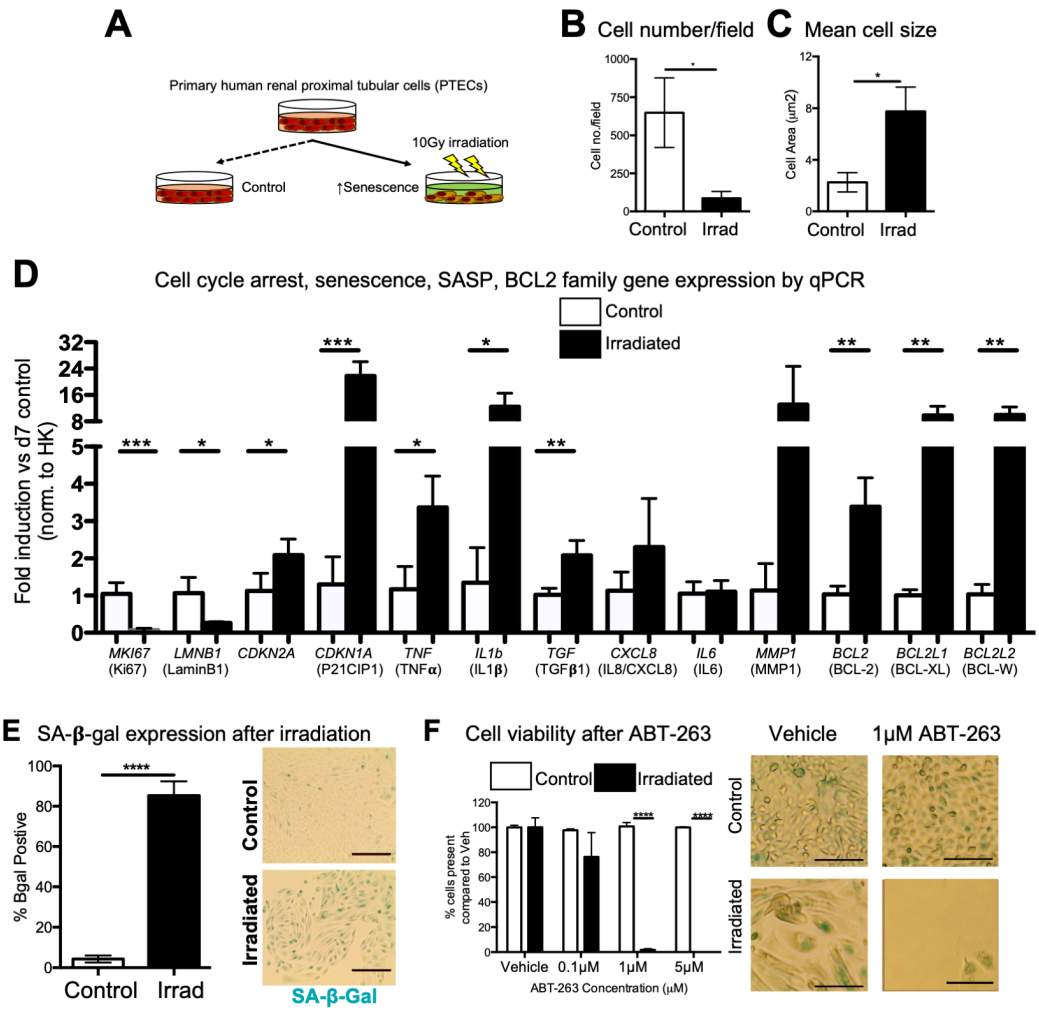
A
Primary human renal proximal tubular cells (PTECs)
10Gy irradiation
Control
↑Senescence
B Cell number/field
Cell no./field
Control
Irrad
C Mean cell size
Cell Area (µm2)
Control
Irrad
D
Cell cycle arrest, senescence, SASP, BCL2 family gene expression by qPCR
Control
Irradiated
Fold induction vs d7 control (norm. to HK)
MKI67 (Ki67)
LMNB1 (LaminB1)
CDKN2A
CDKN1A (P21CIP1)
TNF (TNFα)
IL1b (IL1β)
TGF (TGFβ1)
CXCL8 (IL8/CXCL8)
IL6 (IL6)
MMP1 (MMP1)
BCL2 (BCL-2)
BCL2L1 (BCL-XL)
BCL2L2 (BCL-W)
E SA-β-gal expression after irradiation
% Bgal Postive
Control
Irrad
Control
Irradiated
SA-β-Gal
F Cell viability after ABT-263
Vehicle
1µM ABT-263
Control
Irradiated
% cells present compared to Veh
Vehicle
0.1µM
1µM
5µM
ABT-263 Concentration (µM)
Control
Irradiated

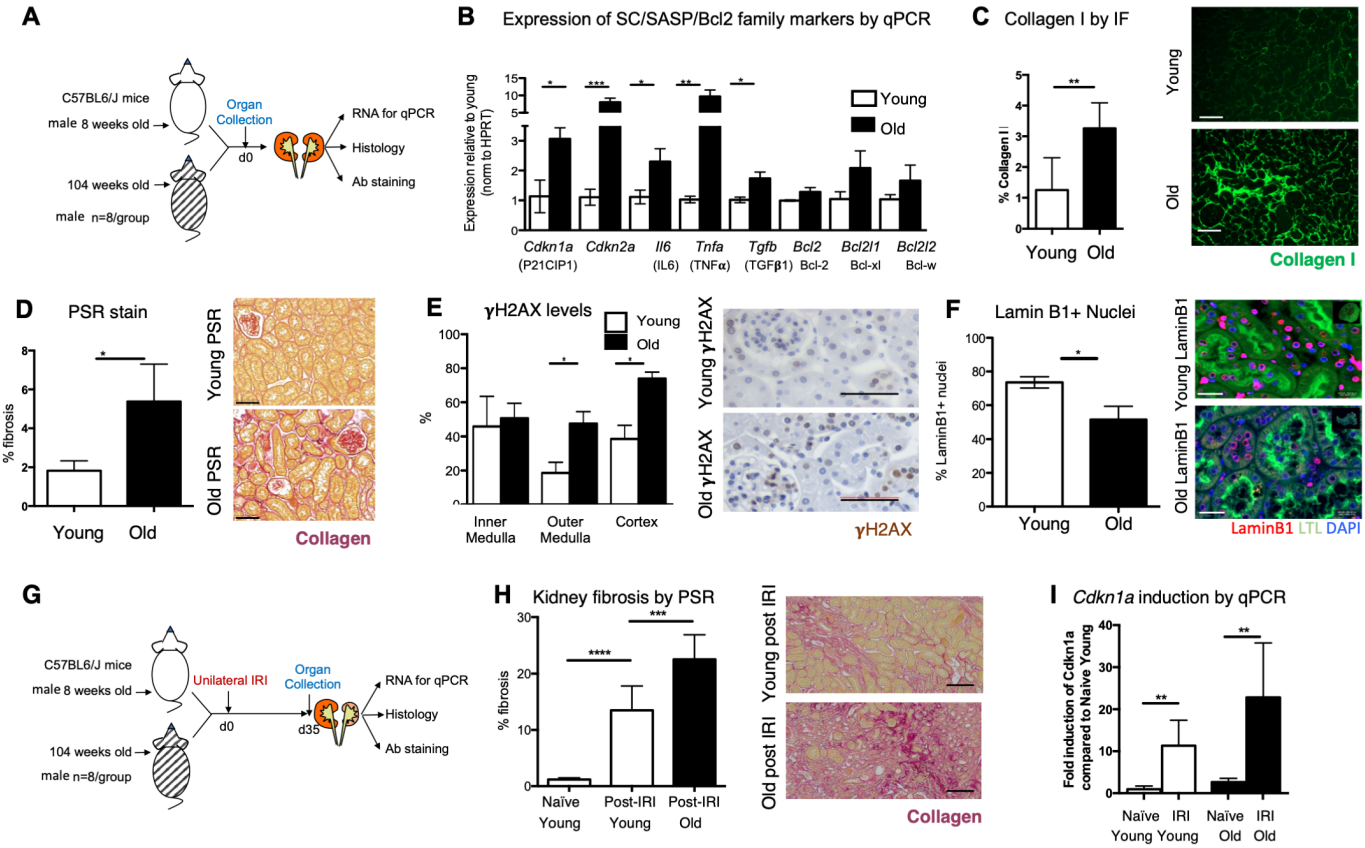
A
C57BL6/J mice
male 8 weeks old
104 weeks old
male n=8/group
Organ Collection
d0
RNA for qPCR
Histology
Ab staining
B
Expression of SC/SASP/Bcl2 family markers by qPCR
Expression relative to young (norm to HPRT)
Young
Old
Cdkn1a (P21CIP1)
Cdkn2a
Il6 (IL6)
Tnfa (TNFα)
Tgfb (TGFβ1)
Bcl2 Bcl-2
Bcl2l1 Bcl-xl
Bcl2l2 Bcl-w
C
Collagen I by IF
% Collagen I
Young
Old
Collagen I
D
PSR stain
% fibrosis
Young PSR
Old PSR
Collagen
E
γH2AX levels
%
Inner Medulla
Outer Medulla
Cortex
Young γH2AX
Old γH2AX
γH2AX
F
Lamin B1+ Nuclei
% LaminB1+ nuclei
Young LaminB1
Old LaminB1
LaminB1 LTL DAPI
G
C57BL6/J mice
male 8 weeks old
104 weeks old
male n=8/group
Unilateral IRI
d0
Organ Collection
d35
RNA for qPCR
Histology
Ab staining
H
Kidney fibrosis by PSR
% fibrosis
Naïve Young
Post-IRI Young
Post-IRI Old
Young post IRI
Old post IRI
Collagen
I
Cdkn1a induction by qPCR
Fold induction of Cdkn1a compared to Naïve Young
Naïve Young
IRI Young
Naïve Old
IRI Old

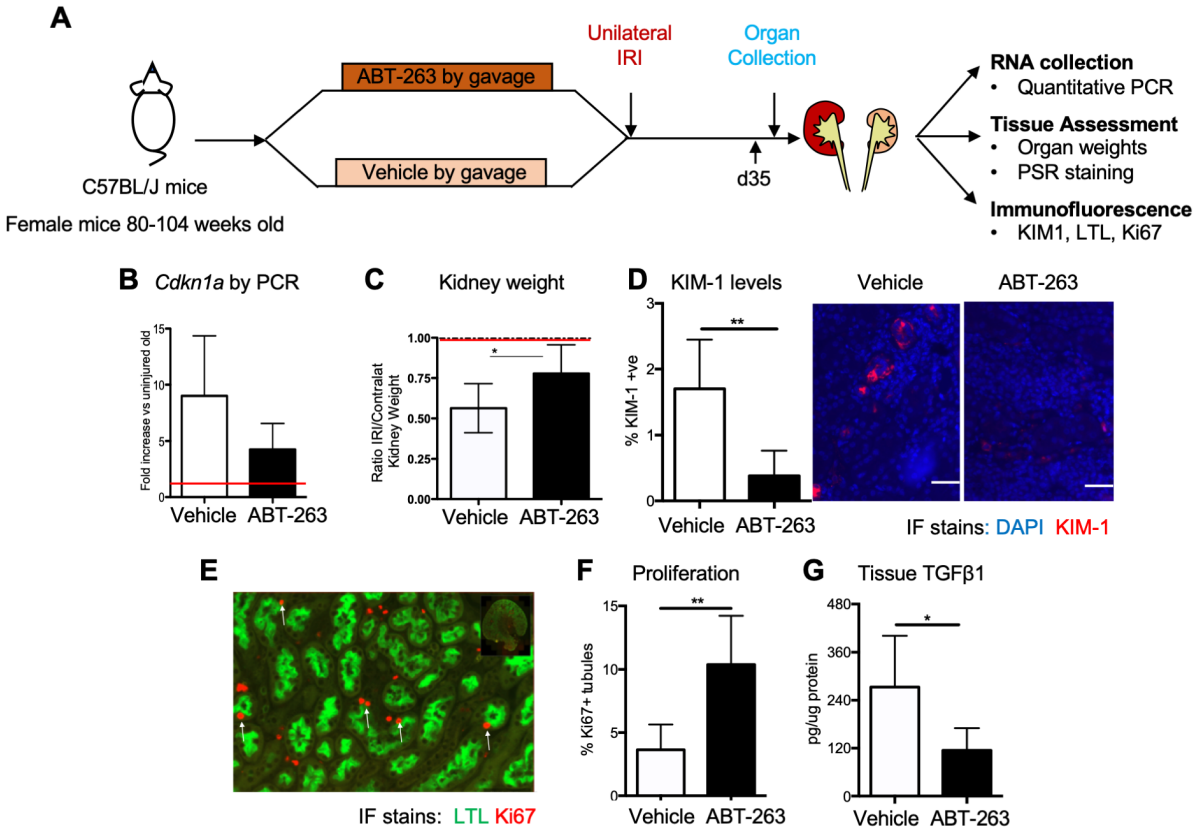
A
Unilateral IRI
Organ Collection
ABT-263 by gavage
Vehicle by gavage
C57BL/J mice
Female mice 80-104 weeks old
d35
RNA collection
• Quantitative PCR
Tissue Assessment
• Organ weights
• PSR staining
Immunofluorescence
• KIM1, LTL, Ki67
B Cdkn1a by PCR
Fold increase vs uninjured old
Vehicle ABT-263
C Kidney weight
Ratio IRI/Contralat Kidney Weight
Vehicle ABT-263
D KIM-1 levels
% KIM-1 +ve
Vehicle ABT-263
Vehicle
ABT-263
IF stains: DAPI KIM-1
E
IF stains: LTL Ki67
F Proliferation
% Ki67+ tubules
Vehicle ABT-263
G Tissue TGFβ1
pg/ug protein
Vehicle ABT-263

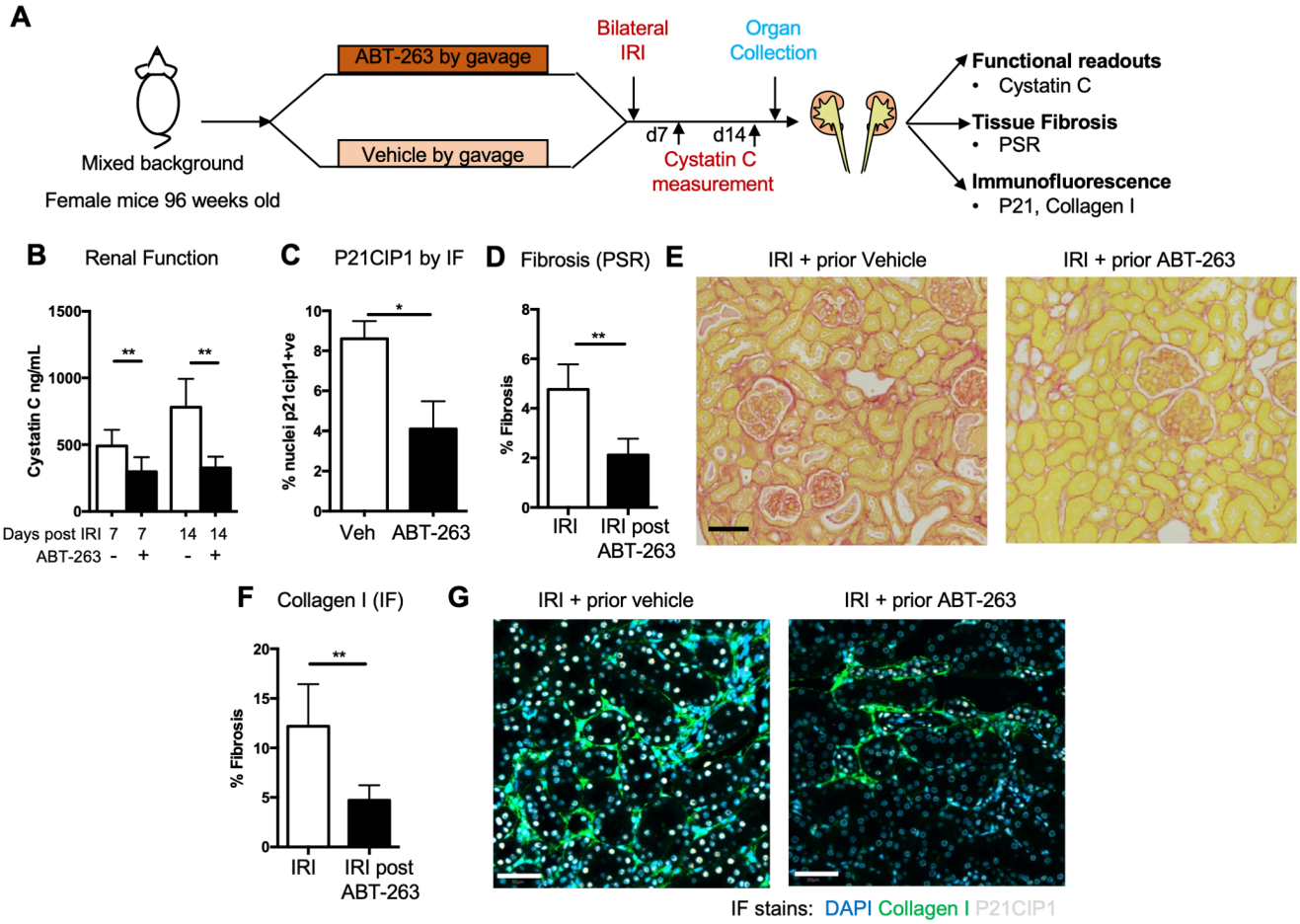
A
Mixed background
Female mice 96 weeks old
ABT-263 by gavage
Vehicle by gavage
Bilateral IRI
Organ Collection
d7
d14
Cystatin C measurement
Functional readouts
• Cystatin C
Tissue Fibrosis
• PSR
Immunofluorescence
• P21, Collagen I
B Renal Function
Cystatin C ng/mL
1500
1000
500
0
**
**
Days post IRI 7 7 14 14
ABT-263 - + - +
C P21CIP1 by IF
% nuclei p21cip1+ve
10
8
6
4
2
0
*
Veh ABT-263
D Fibrosis (PSR)
% Fibrosis
8
6
4
2
0
**
IRI
IRI post ABT-263
E
IRI + prior Vehicle
IRI + prior ABT-263
F Collagen I (IF)
% Fibrosis
20
15
10
5
0
**
IRI
IRI post ABT-263
G
IRI + prior vehicle
IRI + prior ABT-263
IF stains: DAPI Collagen I P21CIP1

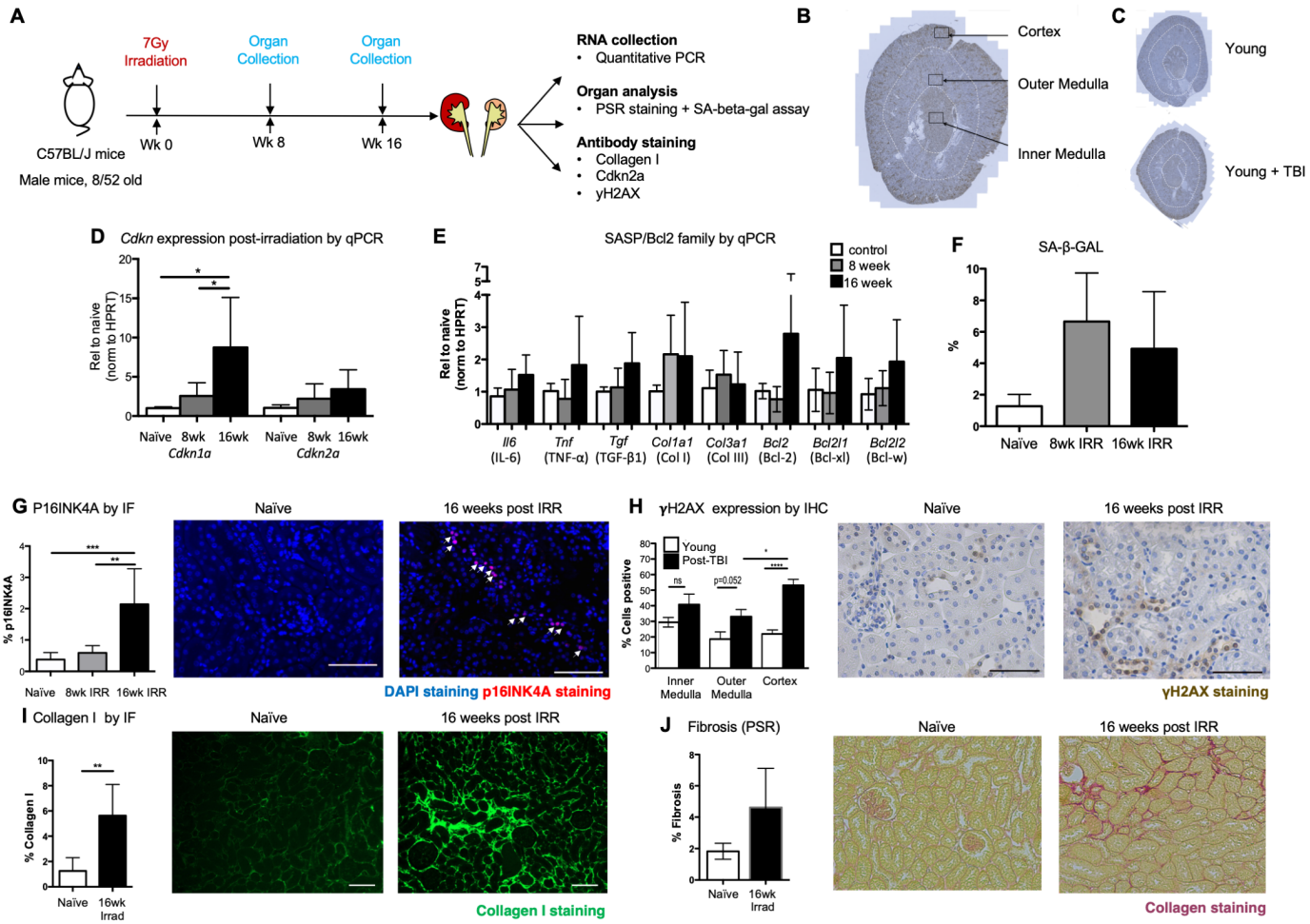
A
7Gy Irradiation
Organ Collection
Organ Collection
C57BL/J mice
Male mice, 8/52 old
Wk 0
Wk 8
Wk 16
RNA collection
• Quantitative PCR
Organ analysis
• PSR staining + SA-beta-gal assay
Antibody staining
• Collagen I
• Cdkn2a
• γH2AX
B
Cortex
Outer Medulla
Inner Medulla
C
Young
Young + TBI
D Cdkn expression post-irradiation by qPCR
Rel to naive (norm to HPRT)
Naïve 8wk 16wk Naïve 8wk 16wk
Cdkn1a
Cdkn2a
E
SASP/Bcl2 family by qPCR
control
8 week
16 week
Rel to naive (norm to HPRT)
Il6 (IL-6)
Tnf (TNF-α)
Tgf (TGF-β1)
Col1a1 (Col I)
Col3a1 (Col III)
Bcl2 (Bcl-2)
Bcl2l1 (Bcl-xl)
Bcl2l2 (Bcl-w)
F
SA-β-GAL
%
Naïve 8wk IRR 16wk IRR
G P16INK4A by IF
% p16INK4A
Naïve 8wk IRR 16wk IRR
Naïve
16 weeks post IRR
DAPI staining p16INK4A staining
H γH2AX expression by IHC
Young
Post-TBI
% Cells positive
ns
p=0.052
Inner Medulla
Outer Medulla
Cortex
Naïve
16 weeks post IRR
γH2AX staining
I Collagen I by IF
% Collagen I
Naïve 16wk Irrad
Naïve
16 weeks post IRR
Collagen I staining
J Fibrosis (PSR)
% Fibrosis
Naïve 16wk Irrad
Naïve
16 weeks post IRR
Collagen staining

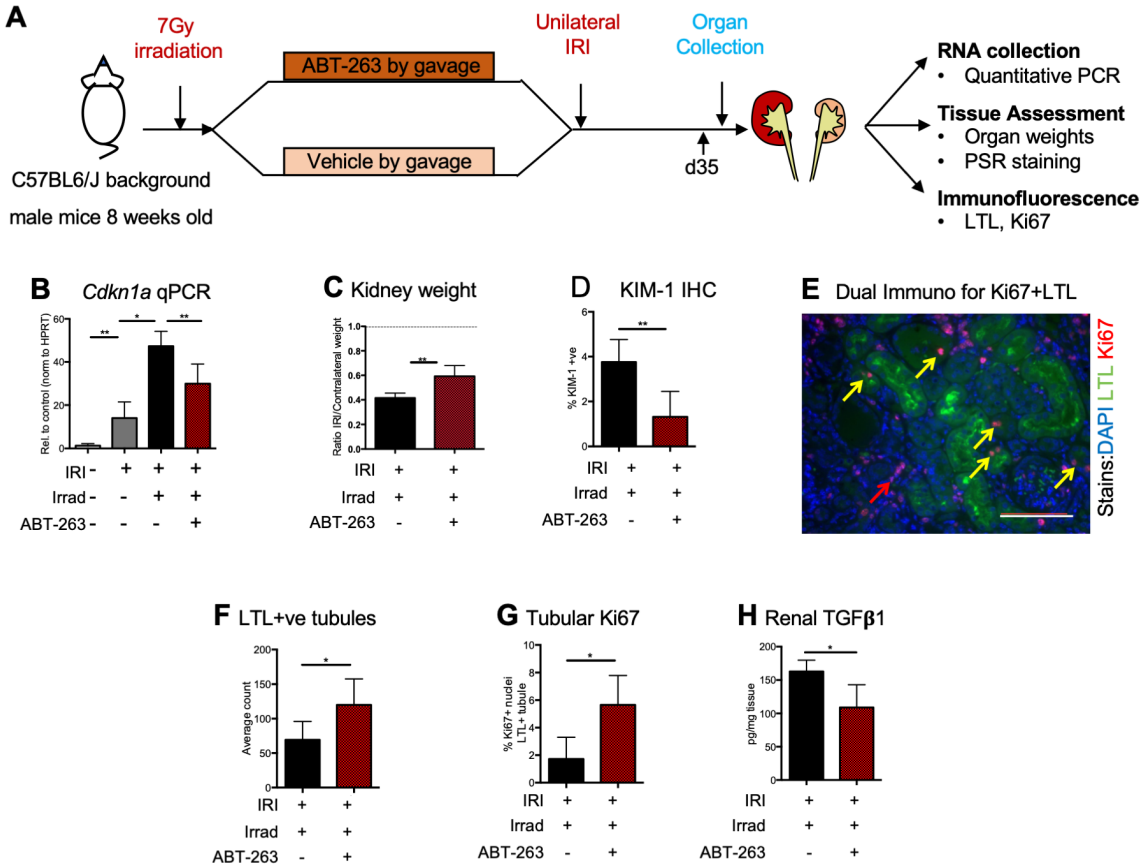
A
7Gy irradiation
ABT-263 by gavage
Vehicle by gavage
Unilateral IRI
Organ Collection
d35
C57BL6/J background
male mice 8 weeks old
RNA collection
• Quantitative PCR
Tissue Assessment
• Organ weights
• PSR staining
Immunofluorescence
• LTL, Ki67
B Cdkn1a qPCR
Rel. to control (norm to HPRT)
C Kidney weight
Ratio IRI/Contralateral weight
D KIM-1 IHC
% KIM-1 +ve
E Dual Immuno for Ki67+LTL
Stains:DAPI LTL Ki67
F LTL+ve tubules
Average count
G Tubular Ki67
% Ki67+ nuclei LTL+ tubule
H Renal TGFβ1
pg/mg tissue
IRI
Irrad
ABT-263

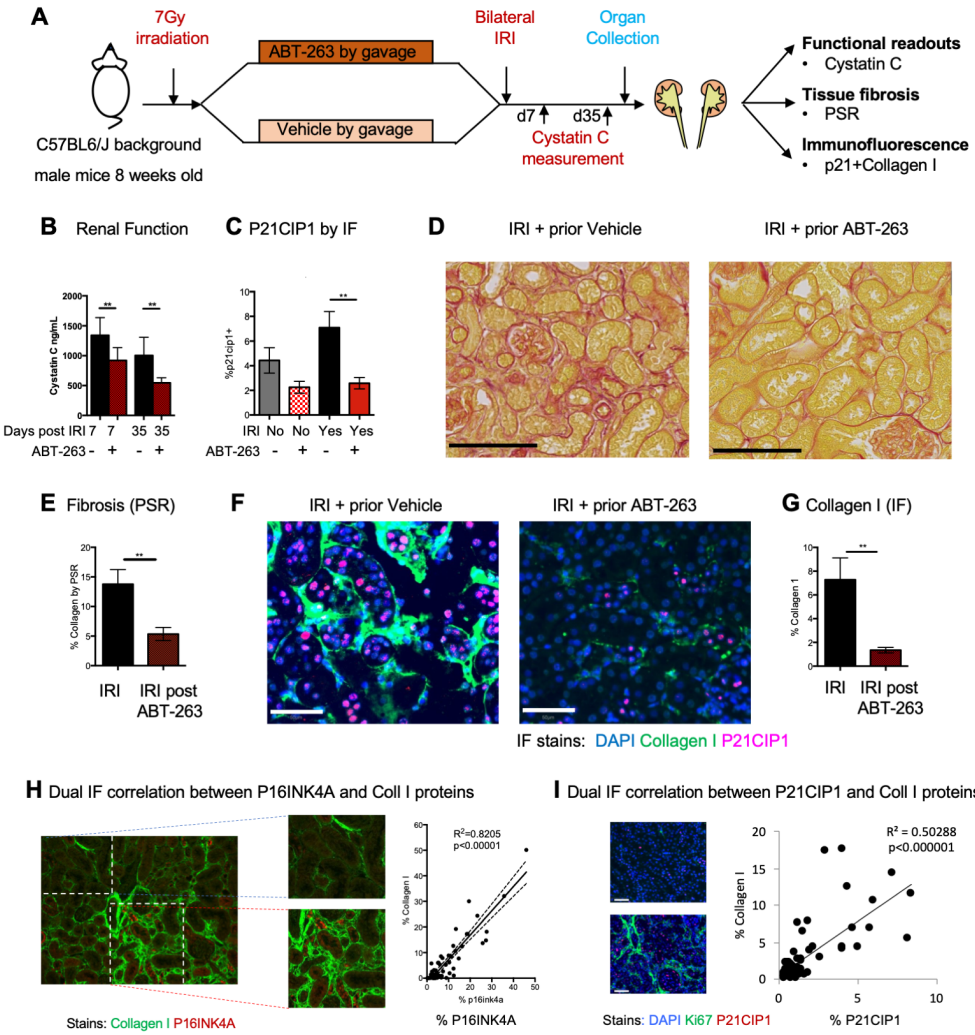
A
7Gy irradiation
ABT-263 by gavage
Vehicle by gavage
Bilateral IRI
Organ Collection
d7
d35
Cystatin C measurement
C57BL6/J background
male mice 8 weeks old
Functional readouts
• Cystatin C
Tissue fibrosis
• PSR
Immunofluorescence
• p21+Collagen I
B Renal Function
Cystatin C ng/mL
Days post IRI 7 7 35 35
ABT-263 - + - +
C P21CIP1 by IF
%p21cip1+
IRI No No Yes Yes
ABT-263 - + - +
D
IRI + prior Vehicle
IRI + prior ABT-263
E Fibrosis (PSR)
% Collagen by PSR
IRI
IRI post ABT-263
F
IRI + prior Vehicle
IRI + prior ABT-263
IF stains: DAPI Collagen I P21CIP1
G Collagen I (IF)
% Collagen I
IRI
IRI post ABT-263
H Dual IF correlation between P16INK4A and Coll I proteins
Stains: Collagen I P16INK4A
R²=0.8205
p<0.00001
% Collagen I
% p16ink4a
% P16INK4A
I Dual IF correlation between P21CIP1 and Coll I proteins
Stains: DAPI Ki67 P21CIP1
R² = 0.50288
p<0.000001
% Collagen I
% P21CIP1

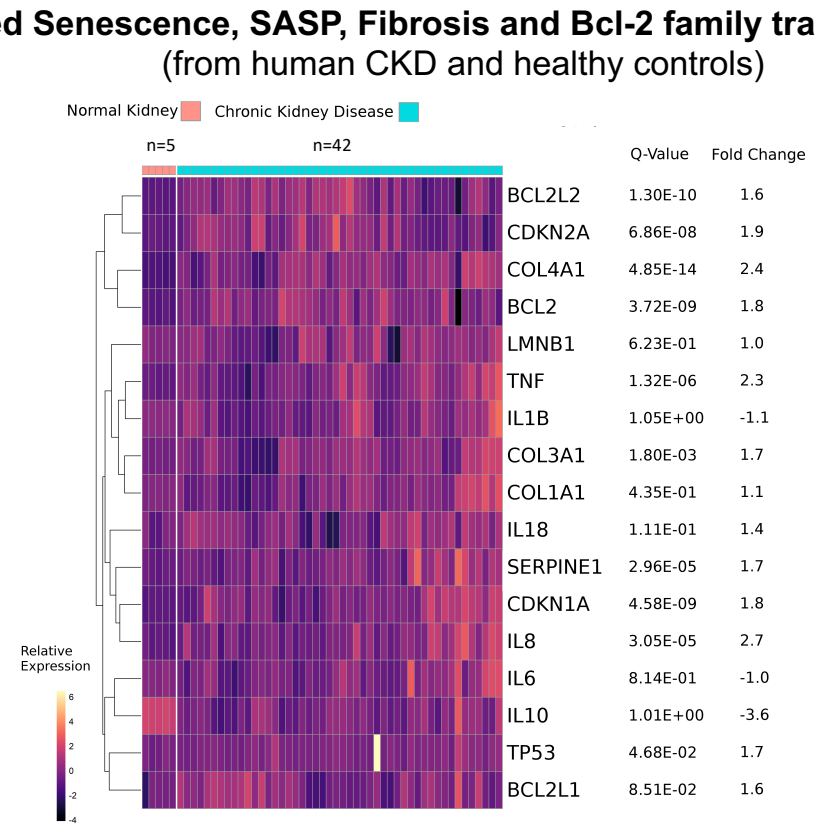


**Figure S1. Expression of selected cyclin dependent kinase inhibitors, SASP factors, fibrotic and Bcl-2 family transcripts detected on microarray analysis in CKD patients and healthy controls, along with adjusted q-values and fold-change (adapted from Nakagawa *et al*(*17*))**

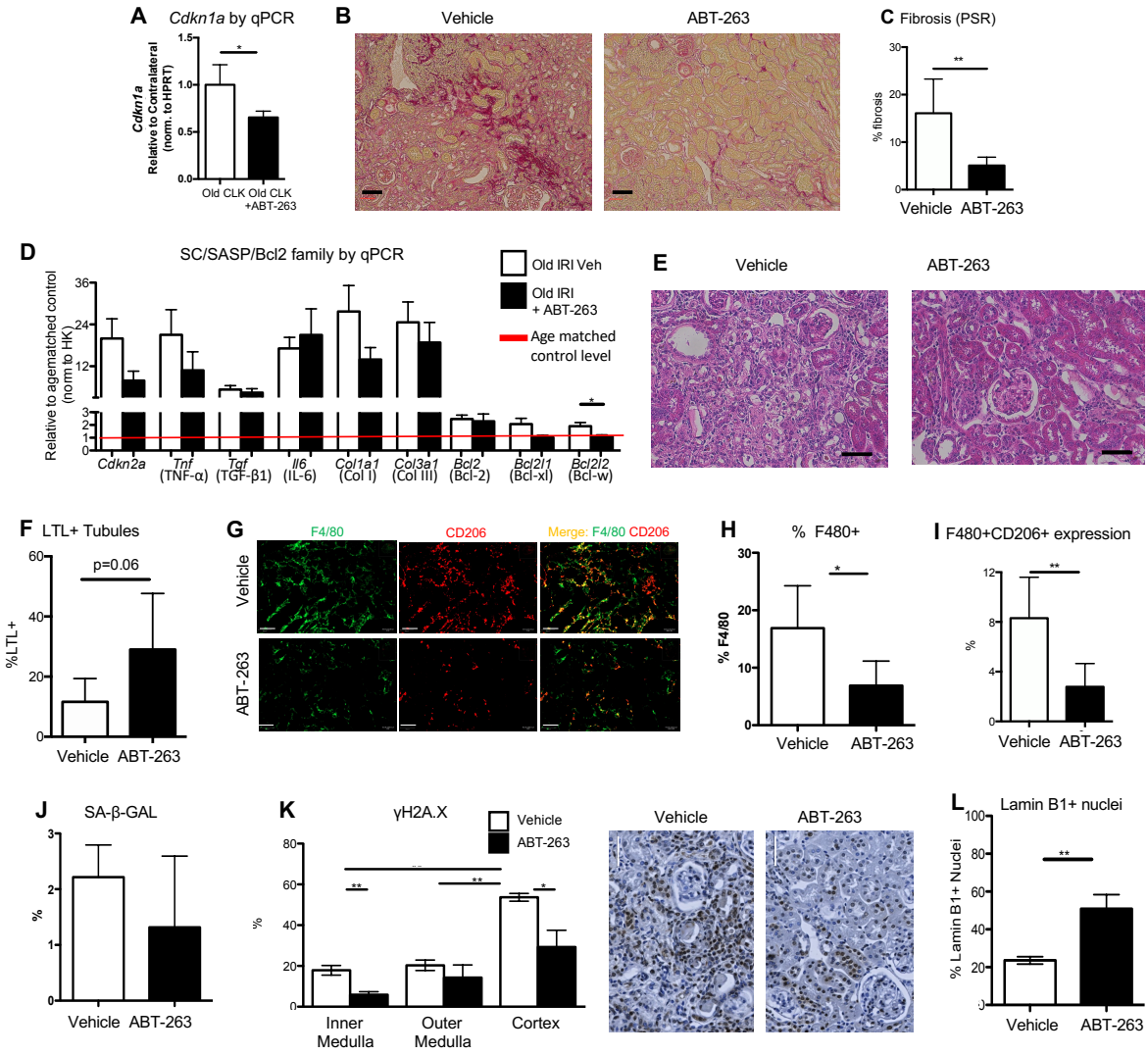


**Figure S2. Pretreatment with ABT-263 in old murine kidneys results in a reduction of fibrosis, DNA damage and macrophages, and favours a reduction of SC/SASP/BCL2 family members and a preservation of LTL+ tubules after injury**. ABT-263 treatment reduces *Cdkn1a* expression in the uninjured kidney (**A**; Mann-Whitney test). Post-IRI PSR IHC (**B**; representative micrographs are shown; 50 μM scale bar), with analysis showing significant reduction in fibrosis in ABT-263 treated animals (**C**). Whole kidney qPCR on samples from old IRI vs old IRI + ABT-263 measuring senescence, SASP markers, fibrosis and BCL2 family members (**D**; red line = expression in old age-matched control tissue) showed that *BCL2L2* (BCL-w) was reduced with ABT-263 treatment (**D**). H&E staining revealed healthier renal architecture in ABT-263 vs vehicle-treated mice (**E**; scale bar represents 50 μM). Staining for

the marker of tubular differentiation (LTL) showed trends toward increase in ABT-263 treated animals (**F**) F4/80 and CD206 double IF was carried out (**G**; representative micrographs are shown; 50 μM scale bar). A reduction in $F4/80^+$ macrophages was measured by IF (**H**). % $CD206^+$ macrophages present in vehicle- vs ABT-263-treated IRI kidneys calculated (**I**). SA-B-Gal staining was carried out between old IRI vs old IRI + ABT-263 (**J**). γH2A.X staining of the kidneys shows evidence of a reduction of DNA damage with ABT-263 treatment after IRI in old mice, most marked in the cortex (**K**). Pre-treatment with ABT-263 in old kidneys increased the proportion of Lamin $B1^+$ tubular nuclei (**L**). Unless otherwise stated comparisons made by unpaired t-test. **P*<0.05, ***P*<0.01. ***P<0.005.

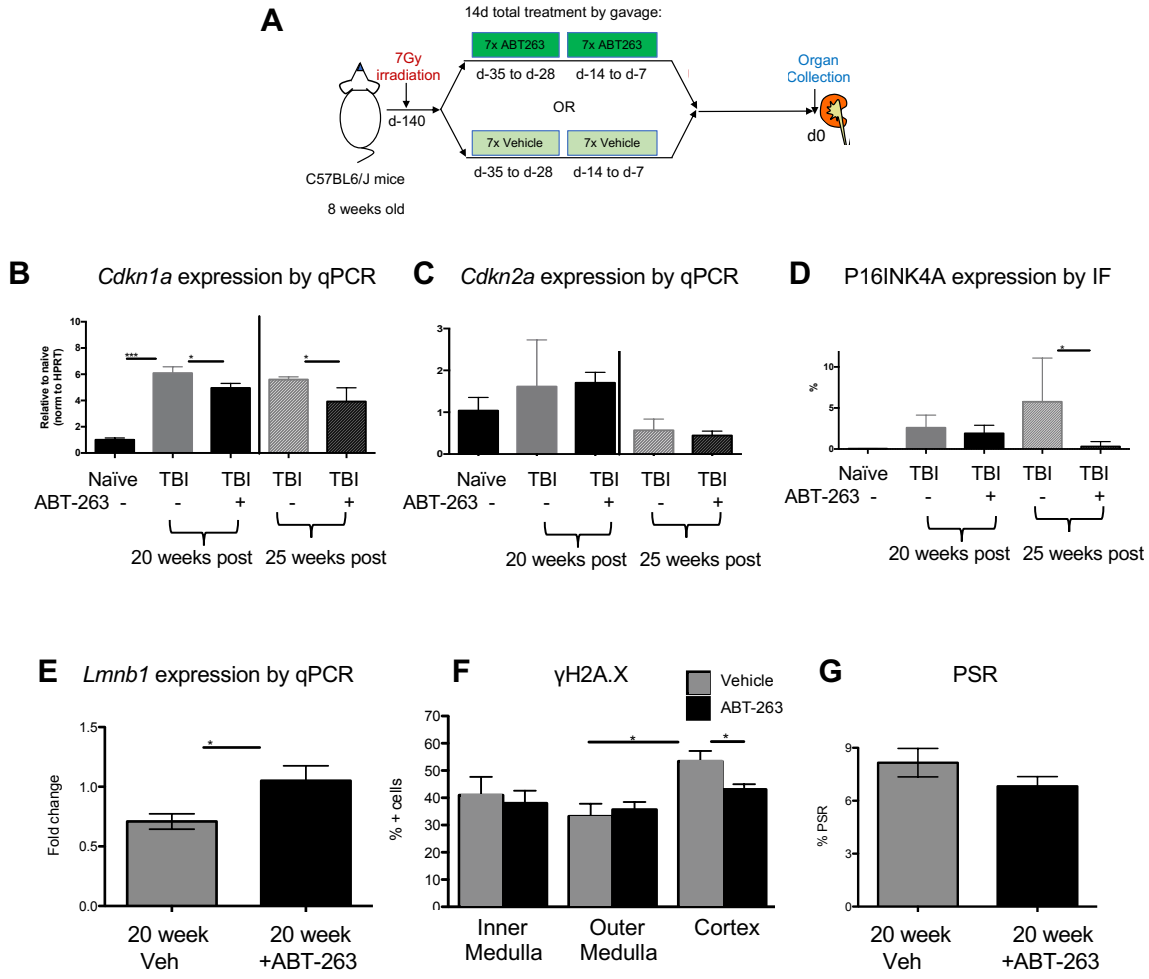


**Figure S3. ABT-263 treatment reduces expression of *Cdkn1a* and *Cdkn2a* transcripts, reduces cortical γH2A.X expression and increases Lamin B1 in the murine kidney.**

TBI at 7Gy was carried out on young mice at day 0, treatment with ABT-263 was at weeks 15 and 18 for 7 days, kidneys were recovered at 20 and 25 weeks (**A**). qPCR was carried out for *Cdkn1a* (P21CIP1; **B**) and *Cdkn2a* (**C**) and IHC for P16INK4A (**D**). At 20 weeks post-TBI, qPCR was also carried out for *Lmnb1* (**E**), as was IHC for γH2A.X staining (**F**) and PSR staining for collagen (**G**). Unless otherwise stated comparisons made by unpaired *t*-test. **P*<0.05, ***P*<0.01. ****P*<0.005.

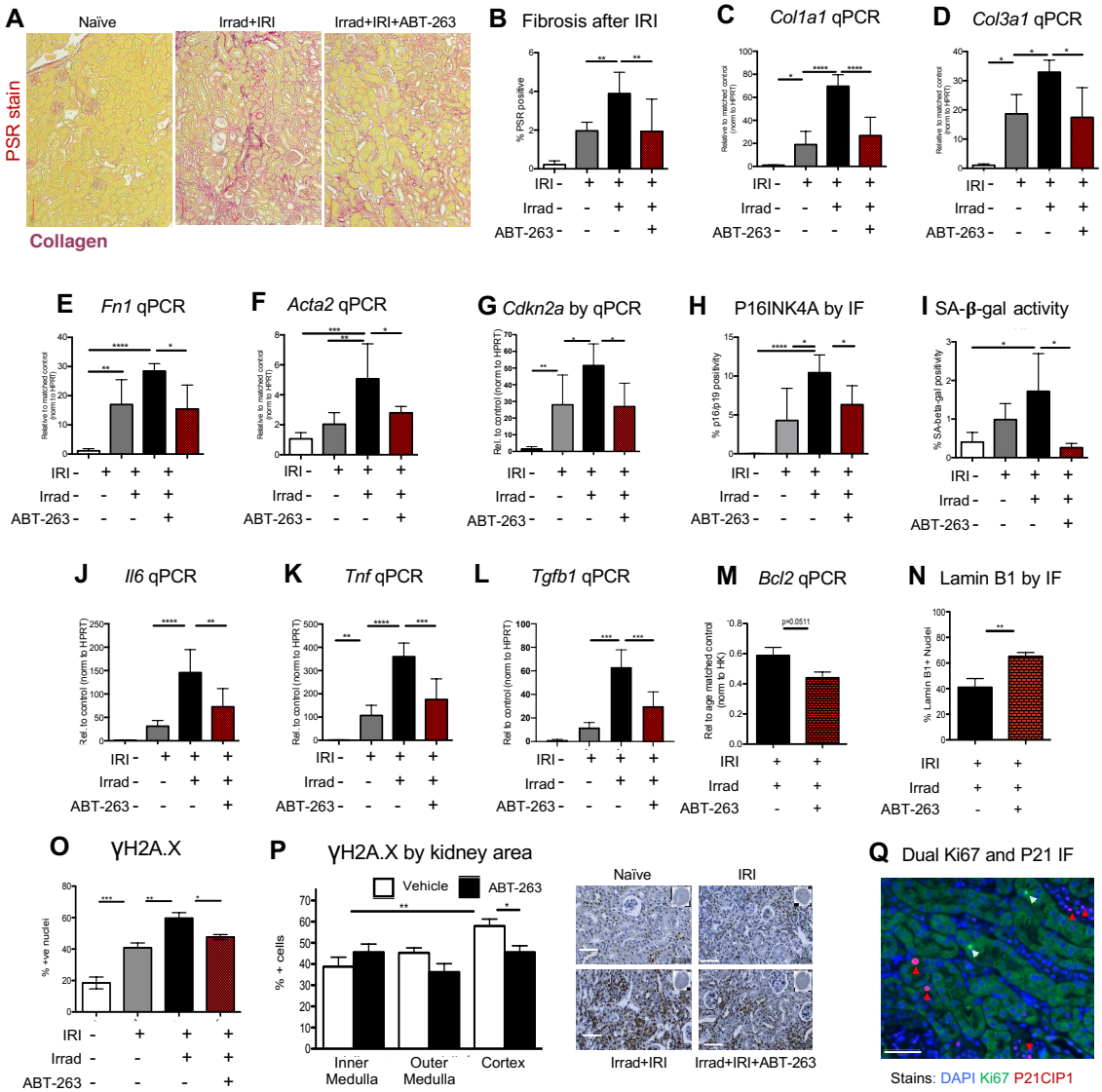


**Figure S4. Irradiation-induced epithelial senescence promotes fibrosis and senescence in murine kidneys with ABT-263 treatment protective.**

PSR staining showed significant reduction in Collagen in ABT-263 pre-treated mice (**A**; representative images, 100 μM scale bar, **B**; comparisons by one-way ANOVA test with Tukey post-test). Fibrosis markers *Col1a1, Col3a1, Fn1* and *Acta2* mRNA showed maximal rises in IRI + irradiation mice, with ABT263 pre-treatment protective (**C-F**). Senescence associated *Cdkn2a* was measured at transcript level by qPCR (**G**), and P16INK4A protein quantified by immunofluorescent staining (**H**; comparisons by one-way ANOVA test with Tukey post-test). SA-B-Gal staining (**I**) and SASP markers *Il6*, *Tnf* and *Tgfb1* (**J-L**) were all augmented in pre-irradiated kidneys + IRI, compared to IRI alone, with ABT-263 pre-treatment normalising the

post-injury expression. qPCR analysis of *BCL2* revealed a decrease between vehicle-treated vs ABT-263-treated pre-irradiated IRI kidneys (**M**). Lamin $B1^{+}$ tubular nuclei were counted comparing vehicle-treated versus ABT-263-treated pre-irradiated IRI kidneys (**N**). γH2A.X staining (**O**) indicated that DNA damage was increased in pre-irradiated kidneys + IRI, compared to IRI alone, with ABT-263 pre-treatment normalising the post-injury expression. Changes in γH2A.X staining were maximal in the cortex, with significant reduction after ABT-263. Representative micrographs are shown (**P**; scale bar represents 50 μM). Dual IF staining for Ki67 and P21CIP1 demonstrated that these markers are mutually exclusive (**Q**, scale bar represents 50 μM). Unless otherwise stated comparisons made by unpaired *t*-test. **P*<0.05, ***P*<0.01. ****P*<0.005.

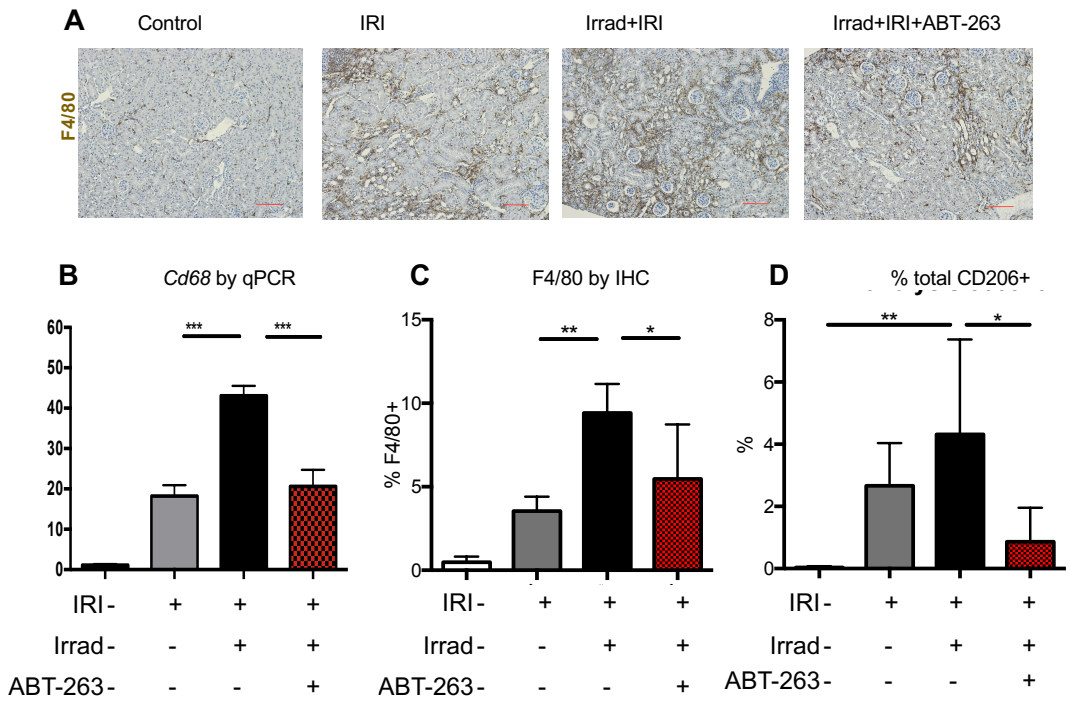


**Figure S5**. **Treatment with ABT-263 alters qPCR and protein markers of macrophage infiltration within the mouse kidney.** *Cd68* qPCR and F4/80 IHC analysis and representative micrographs (**A-C**; 100 µM scale bar). Dual F4/80 and CD206 (MMR) IF analysis showing the % $CD206^{+}$ macrophages present 5 weeks post-IRI (**D**). Unless otherwise stated comparisons made by unpaired t-test. **P*<0.05, ***P*<0.01. ****P*<0.005.

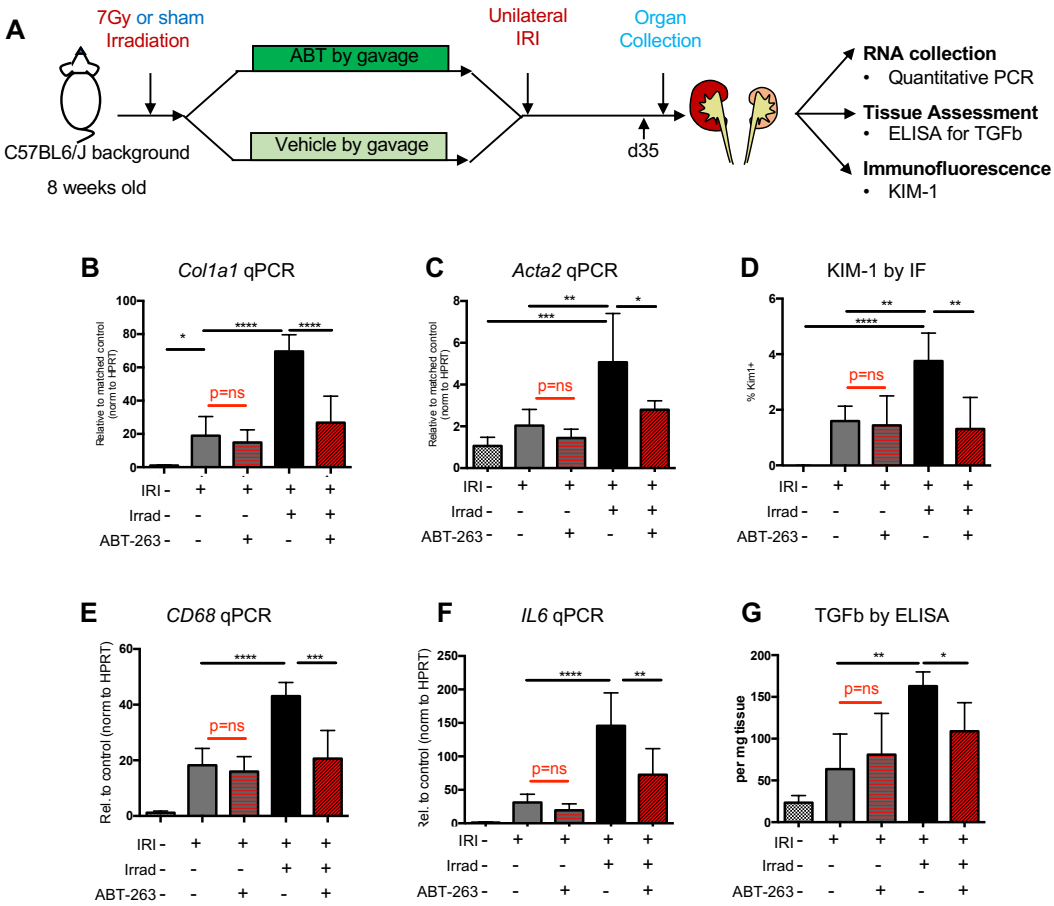


**Figure S6. The efficacy of pre-treatment with ABT-263 is lost in young mice with low quantities of pre-IRI senescent cells.** Young male control mice underwent renal IRI with and without ABT263 and without prior irradiation (**A**). Whilst ABT-263 improved many markers of regeneration in irradiated mice when given prior to IRI, in healthy young mice no protective effect was seen in any assay performed. Plots are shown with equivalent outcomes for *Col1a1* (**B**) and *Acta2* by qPCR (**C**). There was no alteration in KIM-1 by IF (**D**), in macrophage gene expression by qPCR (*Cd68*, **E**), or the key SASP gene *Il6* by qPCR (**F**) or TGF-beta on whole kidney ELISA (**G**). ns=non-significant. **P*<0.05, ***P*<0.01, ****P*<0.005, *****P*<0.001

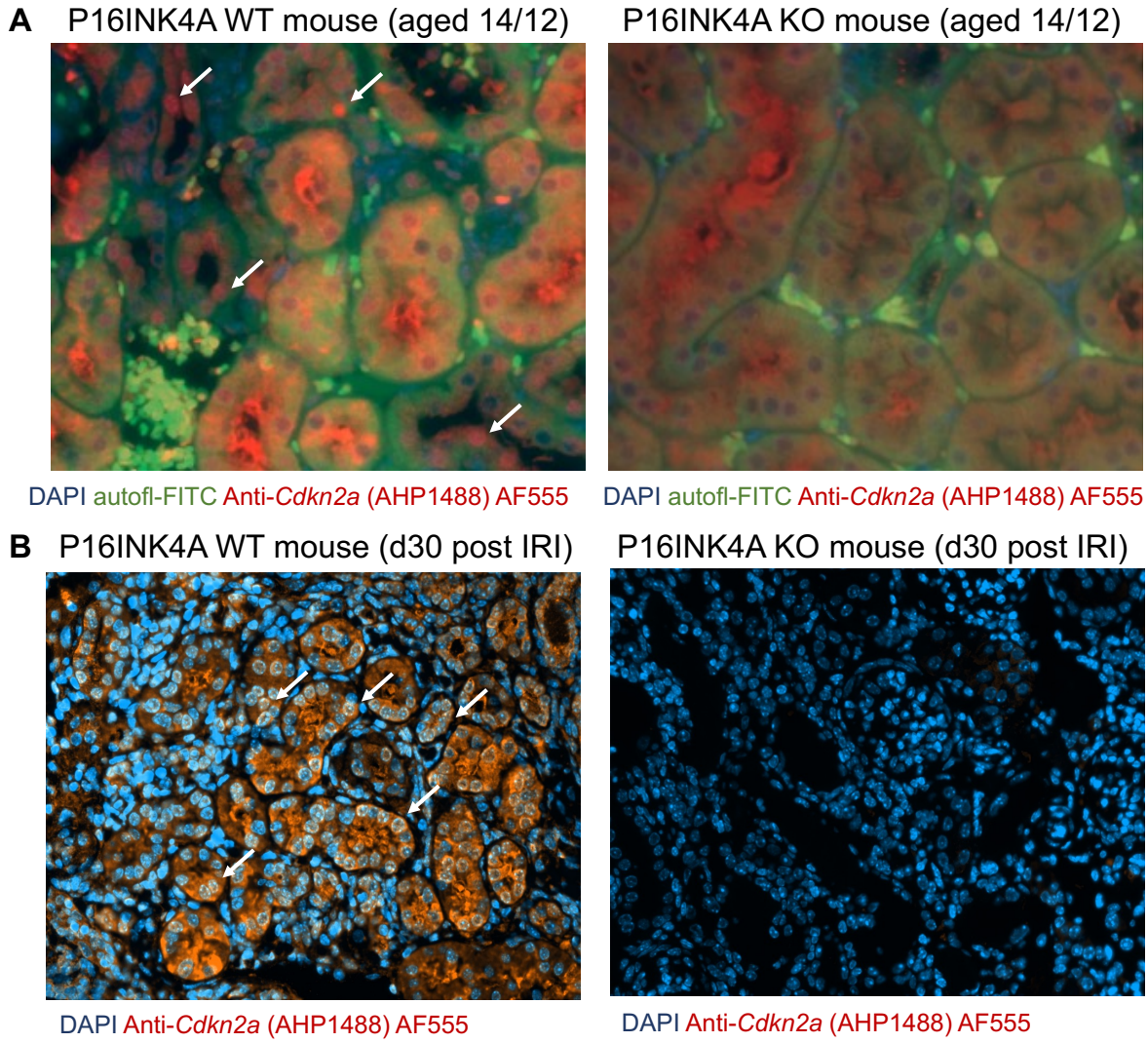


**Figure S7. BioRad Antibody AHP1488 anti-*Cdkn2a* detects P16INK4A but not p19ARF protein expression in aged and fibrotic kidneys.** Kidney samples from naturally aged (14 month) mice or young mice at d30 post renal IRI (with or without a targeted deletion within an exon specific to P16INK4A protein) were stained with AHP1488 (an antibody generated from a P16INK4A protein fragment). Multiple sites of nuclear positivity were seen in aged and fibrotic kidneys from WT mice (**A** and **B, left panels**). In an equivalently aged kidney, or a kidney at the same timepoint after injury with targeted deletion of P16INK4A and preserved p19ARF, no staining was seen (**A** and **B, right panels**). White arrows mark P16INK4A$^{+}$ nuclei.

**Table S1. Multivariate analysis of CDKN1A and CDKN2A and their effect on estimated glomerular filtration rate (egfr) in humans.**

**CDKN1A**

| | | unit | value | Coefficient (univariable) | Coefficient (multivariable) |
|---|---|---|---|---|---|
| **age** | [18.0,73.0] | Mean (sd) | 1.2 (0.9) | 0.03 (0.01 to 0.04, p<0.001) | 0.02 (0.00 to 0.04, p=0.018) |
| **sex** | Female | Mean (sd) | 1.1 (1.0) | - | - |
| | Male | Mean (sd) | 1.2 (0.7) | 0.01 (-0.56 to 0.58, p=0.978) | -0.15 (-0.63 to 0.34, p=0.547) |
| **egfr** | [12.0,299.0] | Mean (sd) | 1.2 (0.9) | -0.01 (-0.01 to -0.00, p=0.001) | -0.01 (-0.01 to -0.00, p=0.049) |
| **Adjusted R-squared = 0.29** | | | | | |

**CDKN2A**

| | | unit | value | Coefficient (univariable) | Coefficient (multivariable) |
|---|---|---|---|---|---|
| **age** | [18.0,73.0] | Mean (sd) | -2.9 (0.3) | 0.01 (0.00 to 0.01, p=0.048) | 0.00 (-0.00 to 0.01, p=0.119) |
| **sex** | Female | Mean (sd) | -2.9 (0.3) | - | - |
| | Male | Mean (sd) | -2.9 (0.2) | -0.03 (-0.21 to 0.14, p=0.714) | -0.05 (-0.23 to 0.13, p=0.571) |
| **egfr** | [12.0,299.0] | Mean (sd) | -2.9 (0.3) | -0.00 (-0.00 to 0.00, p=0.241) | -0.00 (-0.00 to 0.00, p=0.706) |
| **Adjusted R-squared = 0.033** | | | | | |

**Table S2. Primary and secondary antibodies used for IHC and IF**

| Antibody (anti-) | Section Type | Dilution | Company | DAB/IF | Antigen Retrieval | Secondary Antibody |
|---|---|---|---|---|---|---|
| Coll I | MFPE | 1:200 | Southern Biotech | IF | Heat: TE | Anti-goat-AF488 |
| F4/80 | MFPE | 1:50 | AbCam | DAB, IF | Proteinase K (RT) | Biot-anti-rat, anti-rat AF488 |
| γH2A.X | MFPE | 1:100 | AbCam | DAB | None | Biot-anti-rabbit |
| Kim1 | MFPE | 1:50 | R&D | IF | Heat: TE | Anti-goat AF555 |
| Ki67 | MFPE, PFAPE | 1:100 | Cell Sig Tech/AbCam | IF | Heat: TE or CB | Anti-rabbit- or sheep-AF555 |
| LTL-FITC | MFPE | 1:150 | Vector | IF | Heat: TE/CB | None |
| MMR | MFPE | 1:100 | R&D | IF | Proteinase K (RT) | Anti-goat-AF555 |
| P16INK4A | MFPE | 1:100 | BioRad | IF | Heat: TE or CB | Anti-rabbit AF555 |
| P21CIP1 | PFAPE | 1:100 | Abcam | IF | Heat: CB | Anti-rabbit AF555 |
| Lamin B1 | MFPE | 1:100 | AbCam | IF | Heat: CB | Anti-rabbit AF555 |

CB: Citrate buffer; DAB: Diaminobenzidine; IF: Immunofluorescence; IHC: Immunohistochemistry; MFPE: methacarn fixed paraffin embedded; PFAPE: 4%PFA fixed paraffin embedded; RT: Room Temperature. TE: Tris EDTA.

**Data file S1:** Raw data for all figures.